NUREG/CR-3779
SAND83-2579
Vol. 2

The Hydrogen Burn - Equipment Response Algorithm (HYBER)

Reference Manual

Prepared by S. N. Kempka, A. C. Ratzel

Sandia National Laboratories

Prepared for
U.S. Nuclear Regulatory Commission

NOTICE

This report was prepared as an account of work sponsored by an agency of the United States Government. Neither the United States Government nor any agency thereof, or any of their employees, makes any warranty, expressed or implied, or assumes any legal liability of responsibility for any third party's use, or the results of such use, of any information, apparatus, product or process disclosed in this report, or represents that its use by such third party would not infringe privately owned rights.

NOTICE

Availability of Reference Materials Cited in NRC Publications

Most documents cited in NRC publications will be available from one of the following sources:

1. The NRC Public Document Room, 1717 H Street, N.W.
   Washington, DC 20555
2. The NRC/GPO Sales Program, U.S. Nuclear Regulatory Commission,
   Washington, DC 20555
3. The National Technical Information Service, Springfield, VA 22161

Although the listing that follows represents the majority of documents cited in NRC publications, it is not intended to be exhaustive.

Referenced documents available for inspection and copying for a fee from the NRC Public Document Room include NRC correspondence and internal NRC memoranda; NRC Office of Inspection and Enforcement bulletins, circulars, information notices, inspection and investigation notices; Licensee Event Reports; vendor reports and correspondence; Commission papers; and applicant and licensee documents and correspondence.

The following documents in the NUREG series are available for purchase from the NRC/GPO Sales Program: formal NRC staff and contractor reports, NRC-sponsored conference proceedings, and NRC booklets and brochures. Also available are Regulatory Guides, NRC regulations in the *Code of Federal Regulations*, and *Nuclear Regulatory Commission Issuances*.

Documents available from the National Technical Information Service include NUREG series reports and technical reports prepared by other federal agencies and reports prepared by the Atomic Energy Commission, forerunner agency to the Nuclear Regulatory Commission.

Documents available from public and special technical libraries include all open literature items, such as books, journal and periodical articles, and transactions. *Federal Register* notices, federal and state legislation, and congressional reports can usually be obtained from these libraries.

Documents such as theses, dissertations, foreign reports and translations, and non-NRC conference proceedings are available for purchase from the organization sponsoring the publication cited.

Single copies of NRC draft reports are available free, to the extent of supply, upon written request to the Division of Technical Information and Document Control, U.S. Nuclear Regulatory Commission, Washington, DC 20555.

Copies of industry codes and standards used in a substantive manner in the NRC regulatory process are maintained at the NRC Library, 7920 Norfolk Avenue, Bethesda, Maryland, and are available there for reference use by the public. Codes and standards are usually copyrighted and may be purchased from the originating organization or, if they are American National Standards, from the American National Standards Institute, 1430 Broadway, New York, NY 10018.

GPO Printed copy price: $4.50

NUREG/CR-3779
SAND83-2579
Vol. 2

The Hydrogen Burn - Equipment Response Algorithm (HYBER)

Reference Manual

Manuscript Completed: July 1984
Date Published: August 1984

Prepared by
S. N. Kempka, A. C. Ratzel

Sandia National Laboratories
Albuquerque, NM 87185

Prepared for
Division of Engineering
Office of Nuclear Reactor Regulation
U.S. Nuclear Regulatory Commission
Washington, D.C. 20555
NRC FIN A1306

Abstract

The reference guide for HYBER (Hydrogen Burn—Equipment Response), the Hydrogen Burn Survival algorithm, is provided in this report. HYBER is comprised of two self-contained computer programs, DATGEN and SOLVER, developed on VAX 11/780 and CRAY-1 computer systems for use on IBM Personal Computers. These computer codes model single or multiple hydrogen–carbon monoxide–air combustion processes in single-volume vessels, providing predictions for the environment gas state and composition. HYBER was developed to model combustion processes in nuclear reactor containments and to estimate the thermal response of safety-related equipment subject to the combustion and post-combustion environments.

This reference guide discusses the combustion, heat, and mass transfer models included in the algorithm computer codes. The assumptions used in the codes and the execution procedure (i.e., computational framework) in SOLVER are provided. HYBER simulations of two experiments are compared with the data for two different vessels (5.6 m^3 and 2084. m^3 total volume, respectively). These comparisons demonstrate the capabilities of modeling combustion processes with HYBER.

Contents

Figures

Tables

Nomenclature

A	Area	$[m^2]$
B	Mass transfer parameter	
B_{ij}	Beam length between surfaces i and j	$[m]$
C	Drag Coefficient	
C_p	Specific heat at constant pressure	$[J/(kg-K)]$
C_v	Specific heat at constant volume	$[J/(kg-K)]$
e_b	Blackbody emissive power	$[W/m^2]$
D	Diameter	$[m]$
$\mathcal{D}$	Mass diffusivity for steam-air mixtures	$[m^2/s]$
F_{i-j}	Configuration factor between surfaces i and j	
$F_{\Delta\lambda_i T_g}$	Blackbody fraction for gas band i	
g	Gravitational acceleration	$[m/s^2]$
h	Enthalpy	$[J/kg]$
h	Convective heat transfer coefficient	$[W/(m^2-K)]$
h_{fg}	Latent heat of vaporization	$[J/kg]$
k	Thermal conductivity	$[W/(m-K)]$
K	Mass transfer coefficient	$[kg/(m^2-atm-s)]$
L	Characteristic length in convection correlations	$[m]$
M	Mass	$[kg]$
$\dot{M}$	Mass transfer rate	$[kg/s]$
$\overline{MW}$	Molecular weight	$[kg/mole]$
N	Moles	$[moles]$
P	Pressure	$[atm]$
P_{bm}	Logarithmic mean pressure	$[atm]$
q	Heat flux	$[W/m^2]$
$\dot{Q}$	Heat transfer rate	$[W]$
Q	Energy	$[J]$
$\overline{R}$	Ideal gas constant	$[atm-m^3/(mole-K)]$
R	Ideal gas constant	$[J/(kg-K)]$
r	Water droplet radius	$[m]$
S	Distance between points on two surfaces	$[m]$
T	Temperature	$[K]$
T^*	Dimensionless temperature in collision integral	
t	Time	$[s]$
u	Gas speed	$[m/s]$

v	Gas exit speed	$[m/s]$
W	Total thickness of the slab	$[m]$
x	Mole fraction	
z	Slab coordinate	$[m]$

Greek

α	Thermal diffusivity	$[m^2/s]$
α_i	Absorptance for gas band i	
β	Coefficient of thermal expansion	$[1./K]$
γ	Isentropic index	
γ	Stockmayer-potential parameter	
Δm	Mass of droplet evaporated in a time step	$[kg]$
ΔT	Temperature difference	$[K]$
Δt	Time step	$[s]$
Δz	Nodal thickness for material i	$[m]$
ϵ	Gas molecule characteristic energy	$[J]$
ϵ_{w_i}	Emissivity of surface i	
ϵ_{ij}	Gas emittance based on B_{ij}	
θ	Angle with respect to surface normal vector	$[radians]$
κ	Boltzmann's contant	$[J/(molecule - K)]$
μ	Viscosity	$[kg/(m - s)]$
ρ	Density	$[kg/m^3]$
σ	Collision cross-section	$[\mathring{A}]$
τ_{ij}	Gas transmittance based on B_{ij}	
ϕ_{ij}	Function used to obtain gas mixture properties	
χ	Correction for diffusive distortion	
Ω	Collision integral	

Subscripts

a	Air
b	Bulk or average
c	Forced convection
$cond$	Wall condensation
d	Water droplet
e	Exit from control volume
$evap$	Water spray evaporation
fan	Fan flow between upper and lower compartments in ice-condenser PWRs
f	Wall condensate film
g	Gas
i	Gas-liquid interface
in	User-specified
ic	Ice condenser
l	Liquid
$leak$	Leakage out of control volume
nc	Free (natural) convection
net	Summation of net terms
o	Present time step
rad	Radiation
s	Steam
sat	Saturated state
$shock$	Nucleate condensation in supersaturated environment, associated with condensation shock
$spray$	Water sprays
u	Upper compartment of an ice-condenser PWR
w	Wall

Superscripts

$'$	Saturation state or updated condition
$-$	Molar basis or average value
	Time rate of change

Dimensionless Parameters

Fo	Fourier Number, $Fo = \alpha t/D^2$
Nu	Nusselt Number, $Nu = hL/k$
Pr	Prandtl Number, $Pr = \mu C_p/k$
Ra	Rayleigh Number, $Ra = g\beta\Delta TL^3\rho^2/\mu^2$
Re	Reynolds Number, $Re = \rho uL/\mu$
Sc	Schmidt Number, $Sc = \mu/(\mathcal{D}\rho)$

Abbreviations

AIC	Adiabatic Isochoric Combustion
EWB	Exponential Wide Band
FITS	Fully Instrumented Test System
HYBER	Hydrogen Burn—Equipment Response algorithm
NRC	Nuclear Regulatory Commission
NTS	Nevada Test Site
PWR	Pressurized Water Reactor
SNLA	Sandia National Laboratories, Albuquerque, N.M.
TMI – 2	Three Mile Island Unit 2
VGES	Variable Geometry Experimental System

Acknowledgement

This work was performed in support of the Hydrogen Burn Survival (HBS) Program at Sandia National Laboratories, Albuquerque, N.M. The authors acknowledge A. Camp, S. Dingman and M. Wester, members of the HECTR development staff, for their efforts in developing several of the heat transfer models used in the equipment survival algorithm. The authors thank D. King, a member of the HBS project group, for his suggestions for improving HYBER during its development and for his careful scrutiny of the final version. The authors also acknowledge the support of W. McCulloch, project leader of the HBS program.

Executive Summary

The release of hydrogen during a degraded core accident in a nuclear reactor has been recognized as a possible threat to the safe recovery from the accident. The threat is manifested in the possible ignition of the hydrogen, resulting in a high temperature, high pressure gaseous environment. Such an environment could breach the reactor containment or cause thermal damage to safety-related equipment. As part of the reactor licensing procedures, the Nuclear Regulatory Commission requires licensees to provide analyses which show that, in the event of a degraded core accident involving hydrogen deflagrations, combustion-induced damage to the containment and to safety-related equipment will be prevented. To support the NRC review of licensee equipment analyses, the equipment survival algorithm, HYBER (Hydrogen Burn—Equipment Response), has been developed as a part of the Hydrogen Burn Survival program at Sandia National Laboratories, Albuquerque, N.M.

HYBER is comprised of two self-contained computer programs, DATGEN and SOLVER, developed on VAX 11/780 and CRAY-1 computer systems for use on IBM Personal Computers. DATGEN is an interactive computer program which generates the input data files for SOLVER, which performs calculations to simulate combustion and post-combustion phenomena. These codes model single or multiple hydrogen–carbon monoxide–air combustion processes in single-volume vessels, providing predictions for the environment gas state and thermal response of surfaces in and comprising the vessel. The algorithm can be used to support regulatory activities pertaining to the survival of safety-related equipment during hydrogen deflagrations in nuclear reactors. Water spray systems, ice-condenser/fan flow, and gas leakage from containment models have been included in HYBER to facilitate analyses of possible accident scenarios in different reactor geometries.

The reference guide for HYBER is provided in this report. Combustion, heat, and mass transfer models in the computer codes are discussed and the engineering assumptions used in these models are provided. In addition, the execution sequence of the computer program SOLVER is given in detail. Comparisons of HYBER predictions of data from lean hydrogen combustion tests conducted in the FITS vessel (5.6 m^3 volume) and in the NTS dewar (2084. m^3 volume) are also presented. These comparisons demonstrate the capabilities of modeling combustion processes with HYBER. A companion report, the algorithm users guide, describes the usage of HYBER on IBM Personal Computers and discusses the input data generation using DATGEN.

1 Introduction

Since the accident at Three Mile Island Unit 2 (TMI-2), hydrogen generated during degraded core accidents has been recognized as a threat to nuclear reactor containments. The threat is manifested in the possible ignition of the hydrogen, resulting in high pressure, high temperature gaseous products of combustion. Structural failure and subsequent release of radioactive material might result from high pressures, and safety-related equipment might be disabled by large heat fluxes from the high temperature gases. Several schemes to mitigate these effects have been developed such as water-spray cooling and deliberate ignition of low hydrogen concentration mixtures.

As part of reactor licensing procedures, the Nuclear Regulatory Commission (NRC) requires licensees to show that, in the event of a degraded core accident involving hydrogen deflagrations, mitigation systems will prevent damage to equipment that could impair a safe recovery. This is presently done by simulating accident scenarios with one of several computer programs developed for this purpose, most notably, CLASIX, developed by Offshore Power Systems [1]. Typically, heat fluxes predicted in this code are used with thermal conduction models to estimate the thermal response of equipment to the deflagration environment. Another computer program developed to simulate the effects of a degraded core accident is HECTR, developed at Sandia National Laboratories, Albuquerque (SNLA) [2]. HECTR is a large systems code which predicts the thermal environment and thermal responses of nuclear containment surfaces and equipment.

An equipment survival algorithm, HYBER (Hydrogen Burn—Equipment Response) has been developed to support NRC review of equipment survival submittals obtained from codes such as CLASIX and HECTR. The algorithm, developed for the SNLA Hydrogen Burn Survival program, consists of two computer programs named SOLVER and DATGEN. DATGEN is an interactive deck generator (approximately 800 lines of source code) which creates input data files for SOLVER. This supporting code allows the user to select appropriate heat transfer models for various hydrogen deflagration scenarios. SOLVER (approximately 1000 lines of source code) computes the gas environment and thermal responses of equipment and reactor containment walls during hydrogen deflagration scenarios, based on pre-ignition conditions obtained from assumed or predicted scenarios.

HYBER has several advantages which make it appropriate for NRC usage. The algorithm is small and, as a result, executes relatively quickly, which allows the program to be used on personal computers. User-friendly features of HYBER make it useful for performing scoping calculations to predict the consequences of hydrogen deflagrations. HYBER can model deflagrations in any closed, combustion vessel, and thus can be used to model combustion experiments as well as hydrogen deflagrations in nuclear reactor containments.† In addition, the two computer programs are "stand-alone" codes, that is, they require no external libraries and are completely transportable between different computer systems utilizing Fortran 77.

The modeling theory, computational framework, and computing capabilities of SOLVER and DATGEN are described in this document. In addition, a comparison of experimental data with predictions from SOLVER are presented for hydrogen–air combustion tests in intermediate- and large-scale facilities.

†The term "containment" refers to nuclear reactor containments in this report. The terms "vessel" and "enclosure" refer to any confining structure in which a deflagration can occur.

2 Modeling Theory

Many complex physical processes occur during and after hydrogen–air deflagrations within nuclear reactor containments. The degraded core accident sequences which result in hydrogen generation and, in general, define pre-ignition conditions, are not considered here and are not modeled in SOLVER. Such information is usually obtained from other computer programs such as MARCH [3] and is used as input data. The processes of interest are the transport of heat, mass, and momentum in the combustion environment. The next section is a description of these processes, followed by a description of how the processes are modeled in SOLVER.

2.1 Description of Hydrogen Deflagration Phenomena

This section describes the important transport processes which occur during and after hydrogen deflagrations. It is also intended to emphasize the complexity of these processes. Figure 1 shows in schematic the transport processes which determine the rate of change of the gas state and the enclosure wall temperatures. The combustion process releases energy in the form of heat and kinetic energy into the gas. For reactor safety analyses, lean combustion processes are usually considered where ignition criteria and flame propagation processes are not well known, especially in large-scale, reactor containments. For example, large length scales can effect the buoyant acceleration of the flame and combustion completeness, each of which must be known to accurately model the combustion energy release and the combustion-induced gas motion. The gas motion results in forced convection heat transfer between the gaseous combustion products and the walls. After turbulent, viscous effects cause the combustion-induced gas motion to cease, convective heat transport is by means of wall-induced buoyant velocities, referred to as free convection.

Thermal radiation energy transfer results from coupled interchange between the hot combustion products and the surfaces/equipment in the reactor containment. Characterization of the energy transfer for a participating gas medium requires the determination of the gas emittance. This quantity is a function of the gas composition, pressure, and temperature of the non-uniform gas field, and the average "thickness" of the gas which is typically referred to as the mean path

length. For surface interchange, geometrical configuration factors which define how a surface views other surfaces and itself must be known. In addition, the emissivity and reflectivity values for each surface are necessary to completely specify the problem of radiative energy interchange.

Condensation of steam and/or evaporation of water can also occur during a hydrogen deflagration process. The mass transfer rate for condensation on walls is determined by steam diffusion from the combustion gas which depends on the velocity of the gas, the gas composition and state, and the wall temperature. Large heat fluxes on the walls also result from steam condensation in a film-wise or drop-wise mode. Once established, condensate films provide some insulation from convective and radiative heat fluxes on wall/equipment surfaces. Condensation can also occur within the gas by nucleation about suspended particles or if the gas becomes supersaturated. In the event that water-spray mitigation systems are operative, significant gas cooling results from the evaporation of the falling liquid. In each of the above cases, the phenomena are highly transient, coupled heat and mass transfer processes.

Figure 1 indicates that mass and energy transport can also occur via engineering systems and/or structural defects (i.e., leaks), in the enclosure walls. For example, in ice-condenser pressurized water reactors, cool, upper compartment gas is driven into the lower compartment by several large fans. In addition, hot combustion products can expand into the upper compartment via the ice condensers, which cool and remove steam from the gas. Alternate engineering systems such as air coolers and suppression pools are used in other reactor designs. The performance of these systems is dependent on, and is therefore coupled with, the environment.

All of the transport processes described in the preceding paragraphs occur simultaneously and in most cases are highly coupled. Exact evaluation of the processes would require solution of continuity, Navier-Stokes, and energy field equations with constituitive equations for a two phase system including turbulence models. In addition, the inclusion of combustion necessitates solution of chemical-kinetic rate equations. Obviously, solving this system of equations would be difficult in small, well-defined geometries, and prohibitive in complex, large-scale reactor containments. In practice, certain simplifying engineering assumptions are employed to render the problem tractable. Those assumptions used in this work are described in the following section.

2.2 General Engineering Simplifications

The following assumptions are used in HYBER to simplify the analyses associated with modeling combustion and post-combustion phenomena.

- The vessel is comprised of a single, physical compartment. Special assumptions are required to model processes in the lower compartment of ice-condenser pressurized water reactors (PWR). Details are given in Section 3.4.3
- The momentum equation for the gas in the vessel is not solved. When needed, the gas speed is a non-varying, user-specified value which can have different magnitudes during and following combustion.
- Each transport process is quasi-steady, i.e., is constant during each computational time step.
- All deflagrations are global in nature. The duration and completeness of combustion must be known.
- The gas state is uniform throughout the vessel during each time step. This includes gas temperature, pressure and composition.
- Each transport process is treated as an independent phenomenon, thus decoupling all processes.
- Engineering correlations are used to model:

  forced and free convective heat transfer rates

  steam emittance for radiative calculations

  mass transfer rates in analogy with convective correlations

The impact of these general assumptions on the heat/mass transfer processes are summarized in Section 3. Specific assumptions associated with particular heat/mass transfer models are also described in Section 3.

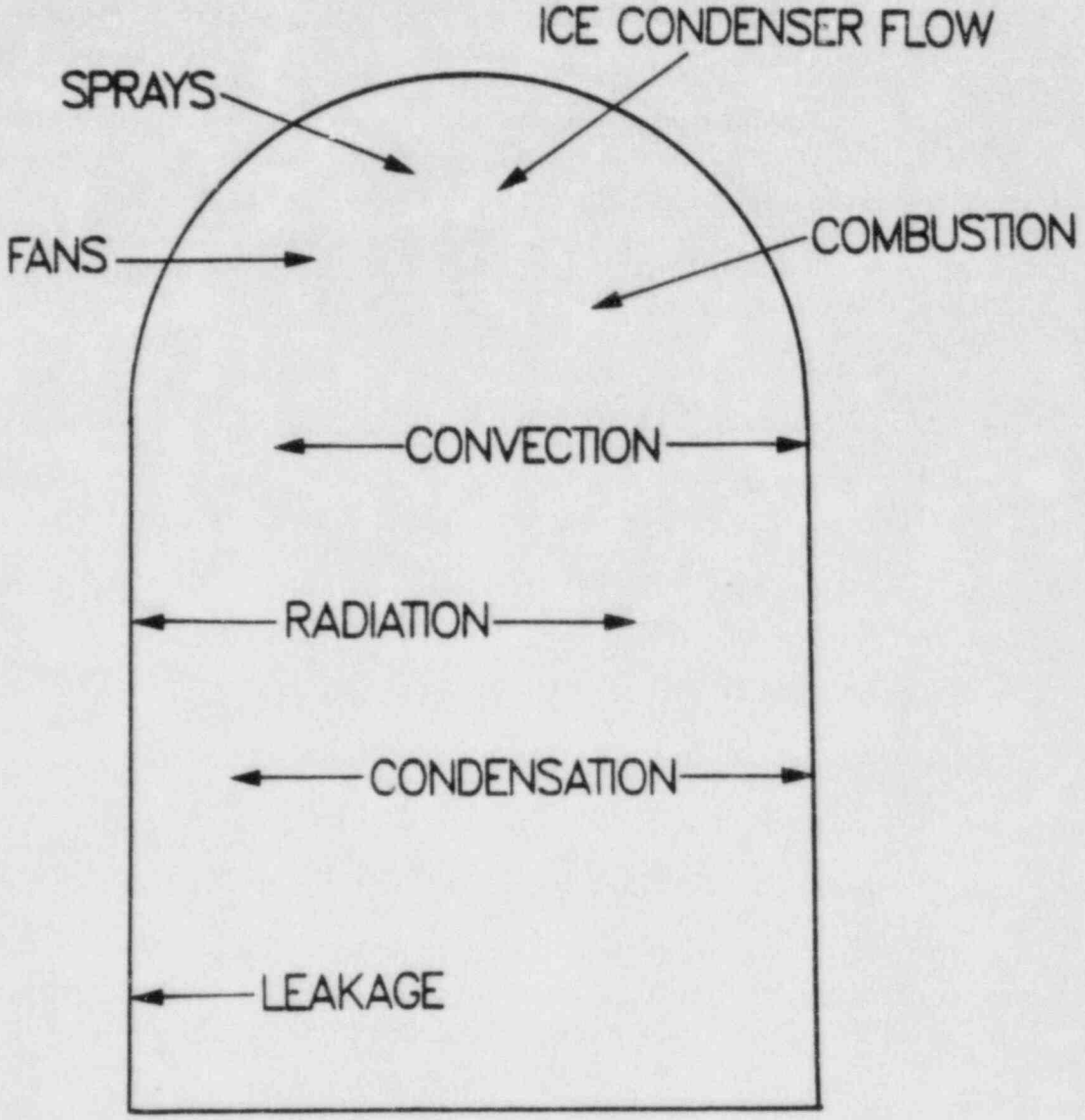

Figure 1. Schematic of heat/mass transport processes resulting from a hydrogen deflagration.

3 Heat and Mass Transfer Models

The heat and mass transfer models used in HYBER are discussed in the following section. This includes a description of the correlations used in the thermal radiation, convection, and condensation heat/mass transfer models. In addition, models for simulating the flow of gas in the lower compartment of ice-condenser PWRs, containment leaks and sprays are given. Thermophysical properties used in heat and mass transfer models are calculated in HYBER. The manner in which the properties are computed is described below.

3.1 Thermophysical Property Determination

Thermophysical properties of gases and water are computed in HYBER using tabulated data and kinetic theory models. Gas mixtures composed of nitrogen, oxygen, carbon monoxide, carbon dioxide, hydrogen, and steam are modeled. The first five gas species are modeled as ideal gases utilizing hard sphere models to compute gas thermal conductivities and viscosities. Thermal conductivity and viscosity values for steam are also obtained using hard sphere models (including polar molecule effects) when the gas temperature is greater than 2530 K. At lower temperatures, tabulated properties are used which account for non-ideal gas behavior. All gas specific heats at constant pressure are obtained from polynomial fits of specific heat data compiled in the JANAF tables [4]. When computing the specific heat at constant volume, ideal gas behavior is assumed for each of the constituents and Eq.(1)† is used.

$$\overline{C}_v = \overline{C}_p - \overline{R} \tag{1}$$

Specific formulations for the thermal conductivity and viscosity models are given in Reid, Prausnitz, and Sherwood [5]. These equations are

†All variables used in this report are defined in the Nomenclature. Where appropriate, terms are defined in the text.

$$\mu = 2.669(10^{-6}) \frac{\sqrt{\overline{MW}T_g}}{\sigma^2 \Omega}, \tag{2}$$

and

$$k = 4.186(10^3) \frac{\mu}{\overline{MW}}(3.52 + 1.32\overline{C}_v), \tag{3}$$

where

$$\Omega = \frac{1.16145}{T^{*0.14874}} + \frac{0.52487}{\exp(0.7732T^*)} + \frac{2.16178}{\exp(2.43787T^*)} + \frac{2\delta^2}{T^*} \tag{4}$$

and

$$T^* = \frac{\kappa T_g}{\epsilon}. \tag{5}$$

The viscosity is obtained using the Chapman-Enskog viscosity equation while the thermal conductivity is given by a modified Eucken model. The Lennard-Jones potential function is used to formulate the collision integral. The Stockmayer correction is included in the collision integral to account for the steam molecule polar effect. Computed values for thermal conductivity and viscosity are within $\pm 5\%$ of experimentally measured properties for pure gases. This variation is acceptable given all other uncertainties associated with obtaining a correct temperature to use in these models.

Mixture theory models based on mole fraction weighting, as recommended in reference [5], are used to obtain the thermophysical properties for mixtures of gases. The specific heat at constant pressure and the average molecular weight are obtained using a direct mole fraction weighting given in Eq.(6).

$$\overline{A} = \sum_{i=1}^{G\,gases} A_i x_i \tag{6}$$

The molecular weight or specific heat is given by A_i and x_i is the mole fraction. The subscript "i" refers to species i.

The Chapman-Enskog theory is applied to obtain a gas mixture viscosity given by Eq.(7). The function is obtained using Wilke's approximation, shown in Eq.(8).

$$\mu_g = \sum_{i=1}^{G\,gases} \frac{\mu_i x_i}{\sum_{j=1}^{G\,gases} x_i \phi_{ij}} \tag{7}$$

and

$$\phi_{ij} = \frac{[(1+\mu_i/\mu_j)^{0.5}(\overline{MW_j}/\overline{MW_i})^{0.25}]^2}{[8(1+\overline{MW_i}/\overline{MW_j})]^{0.5}}, \tag{8}$$

where $\overline{MW_i}$ and μ_i are the molecular weights and viscosities, respectively, for gas species i.

The thermal conductivity for a gas mixture is also obtained using Eqs.(7) and (8), replacing the viscosity with the thermal conductivity for each gas specie. This latter model is known as the Wassiljewa equation and incorporates the Mason and Saxena modification for ϕ_{ij}. Refer to reference [5] for additional details on these models.

All thermophysical properties of water used in spray and condensation models, except for the saturation pressure, are tabulated. The saturation pressure is given by a polynomial function of temperature [6]. Tabulated properties are density, thermal conductivity, viscosity, and heat of vaporization, all of which are given in terms of temperature. Saturation temperature versus pressure is also tabulated. Diagnostics are also included in this package to indicate when the data are outside of the tabulated range.

The gas and water property evaluation package executes quickly and occupies minimal space in HYBER which facilitates its use on a personal computer. Although efficient, this package uses between 20-40 % of the CPU time in an equipment survivability calculation. This might be reduced by inclusion of tabulated values for the Lennard-Jones collision potential function needed in the viscosity evaluation.

3.2 Combustion Model

Combustion processes are modeled in the algorithm in two steps. During the generation of a data file (using DATGEN), the user is prompted to perform an adiabatic isochoric (constant volume) combustion (AIC) calculation. Note that only global deflagrations are considered in HYBER. Results from this calculation are used in SOLVER, either as initial conditions if the combustion is to be modeled as an adiabatic process, or to determine the energy released and the change in gas composition during the burn. Specific details pertaining to these different options are described in the sections to follow.

3.2.1 Combustion Calculations in DATGEN

Combustion calculations in DATGEN are performed using an adiabatic isochoric combustion routine developed by Baer and Ratzel for a hydrogen flame propagation model [7]. Hydrogen–air and carbon monoxide–air deflagrations are considered in this routine incorporating the following chemical processes.

$$H_2 + 0.5O_2 \leftrightarrow H_2O$$

$$OH + 0.5H_2 \leftrightarrow H_2O$$

$$2H \leftrightarrow H_2$$

$$2O \leftrightarrow O_2$$

$$NO \leftrightarrow 0.5N_2 + 0.5O_2$$

$$CO + 0.5O_2 \leftrightarrow CO_2$$

Appropriate coupled relations for these processes include the chemical kinetics rate equations and energy balances associated with the reactions. Data for the equilibrium constants and for the internal energies of the eleven gas species are obtained from the JANAF tables [4] and are given as a function of temperature. Since the combustion is assumed to be confined (constant volume), the expansion ratio is unity and the final gas pressure, temperature and composition

are determined. Since this is an AIC calculation, the final temperature and pressure represent upper bounds for the actual combustion process which would occur in the vessel. Generally, energy would be lost from the combustion products to the cooler walls during a deflagration, resulting in lower peak temperatures and pressures. Note that in this calculation it is also assumed that the initial and final gas states represent some mean state of the gas. Thermal stratification in the enclosure is not considered and the gas composition is assumed to be uniform throughout combustion.

Hydrogen–air deflagrations can be modeled as either complete or incomplete combustion processes while carbon monoxide–air deflagrations are always assumed to be complete. A complete combustion process consumes all available fuel, whereas an incomplete process consumes only a fraction of the fuel. When an incomplete hydrogen–air deflagration is modeled, the user must specify the fraction of hydrogen that is to be consumed. The remaining hydrogen is treated in the combustion calculation as an inert gas which serves as a diluent. In addition, the effect of water sprays on the combustion process can be included by modeling water suspended in the gas. The water serves as a heat sink which absorbs some of the released combustion energy. Suspended water first saturates, then evaporates and finally superheats to the final gas state. Appropriate spray system parameters including the spray injection rate, spray droplet sizes and distribution, and fall distance are required so that the quantity of water suspended in the gas can be estimated. Note that the inclusion of water will decrease the final gas temperature and pressure while increasing the steam concentration. The results of calculations performed which include suspended water are meant only to provide some estimate of the final conditions. The final AIC results which are provided to SOLVER are those conditions which result from a no-sprays-on AIC calculation. This means that the effect of sprays on the combustion processes are actually modeled in SOLVER using the spray model to be described in Section 3.4.1.

The combustion model included in DATGEN can be used to directly obtain the gas state at the end of combustion (hereafter referred to as the final gas state) given an initial gas composition and state. It can also be used to match some desired final state which has been predicted by computer codes such as CLASIX. In the latter case, DATGEN prompts the user to decide if the calculated final state following combustion is comparable. If not, then the user can alter the gas composition, the hydrogen–air combustion completeness, and/or the water spray parameters to effect the final combustion results. Once the user is satisfied with the final, calculated gas state, it is saved for use in SOLVER. It should again be noted that the temperature and pressure obtained in DATGEN are upper bounds associated with adiabatic combustion. If the user wishes to model heat

losses during combustion, then he should select a final AIC state in excess of the conditions which he would like to match at the completion of combustion. The final state computed in SOLVER will be less than the AIC state when the combustion is non-adiabatic because the gas will lose energy to the vessel walls and equipment during combustion.

Heat and mass transfer during the deflagration can only be modeled in SOLVER. In this case, the user must specify (in DATGEN) an effective burn length and some mean burn velocity which are used to determine the combustion duration. These data are used with the final gas state to simulate the deflagration in SOLVER.

3.2.2 Combustion Simulation in SOLVER

If specified by the user, heat and mass transfer can be modeled in SOLVER during combustion. Otherwise, the combustion is adiabatic, and the AIC conditions computed in DATGEN are used as the initial gas conditions for the simulation of the post-combustion heat/mass transfer analyses.

Combustion analyses in SOLVER use the initial gas state and final AIC gas state provided from DATGEN. In the absence of heat and mass transfer, combustion is assumed to increase the gas temperature and modify the appropriate gas species linearly between the initial and final combustion conditions over the user-prescribed combustion time. The inclusion of heat and mass transfer during combustion, however, results in a nonlinear gas temperature, pressure, and composition. When included, gas expansion and leakage also change the gas composition during combustion. The time for combustion completion is also important in this analysis, since the heat loss rate integrated over time yields the energy lost from the gas. Thus, fast combustion processes will yield a final gas state near the AIC conditions because there is little time for energy losses to occur. The gas pressure is obtained from the ideal gas equation of state.

If the leak or expansion models are incorporated in a non-adiabatic combustion process, it is assumed that the fuel to be combusted cannot be vented during combustion. This constraint is necessary to assure that the combustion conditions selected in DATGEN can be met. In such cases, the final gas temperature and fuel composition will be near the AIC results predicted in DATGEN, and the gas pressure and non-fuel composition will be reduced owing to the venting process

3.3 Models of Heat/Mass Transfer Mechanisms

3.3.1 Radiation Model

The radiation model included in SOLVER allows for energy transfer between the surfaces and between the steam participating medium. Since the gas in the enclosure is assumed to be isothermal and uniform in species composition, a single gas volume element can be modeled. When no steam is present in the vessel, the radiation model discussed in this section reduces to the radiative surface interchange problem through a transparent non-attenuating gas medium. The gas emittance correlation used in the algorithm and the enclosure model are described in the following sections.

Gas Emittance Model

From a radiative energy transfer standpoint, steam is the most important gas species that is present in a reactor containment during a degraded core accident. Steam can be released directly into the containment as the moderator coolant water is vaporized during the accident, or it can result as a product of a hydrogen–air deflagration. Other gases typically found in containment such as nitrogen, oxygen, and the inerts found in air do not act as participating species in radiative exchange. That is, these gases do not emit nor absorb radiative thermal energy. A gas mixture comprised solely of these gas species is said to be transparent. Steam, on the other hand, absorbs and emits thermal radiative energy over five specific spectral regions denoted as bands, with centers of absorption located at 10-20 μm (rotational), 6.3 μm, 2.67 μm, 1.87 μm, and 1.38 μm [8]. All other spectral regions in the steam wavelength spectrum are transparent.

The absorbing-emitting steam gas-bands can be thought of as regions where the gas is nearly opaque. That is, radiative energy (photons) with appropriate energy levels passing through a steam-laden gas would be absorbed by these gas bands. The steam would also emit photons with energy levels associated with these bands. The relative importance of the different absorption-emission bands depends upon the gas temperature. At lower temperatures, the gas absorbs/emits radiative energy in/from the longer wavelength bands (principally the rotational and 6.3 μm bands). At elevated temperatures associated with times around combustion, the 2.67 μm band becomes important. The gas temperature must be in excess of 1500 K before the 1.38 μm and 1.87 μm steam bands are critical to the radiative computations.

Absorption and emission properties of a gas can be characterized by the gas emittance which is an integrated value typically computed as shown in Eq. (9), where $\overline{\alpha}_g$ is a mean value of absorptance for a particular gas band and $F_{\Delta\lambda_i T_g}$ is a blackbody weighting function [8].

$$\epsilon_g = \sum_{i=1}^{I\ bands} \overline{\alpha}_g F_{\Delta\lambda_i T_g} \tag{9}$$

The different band absorptances depend upon not only the particular nature and quantity of the radiating gas, but also on the total gas composition, on the gas temperature and pressure, and on the effective radiating distance. The latter dependence is a function of the geometry and is typically referred to as the effective "path" or "beam" length. A formal definition of the beam length as used in this work is given below,

$$B_{ij} = \frac{1}{A_i A_j} \int_{A_i} \int_{A_j} S dA_i dA_j, \tag{10}$$

where S is the distance between points on the two surfaces of areas A_i and A_j.

Representative beam-length data for simple geometries are given in references [8,9], and the reader is referred to these sources for assistance in computing beam lengths. An additional description of the beam-length concept is provided in the users' manual for HYBER [10]. It also describes the reciprocity relations required for beam-length inputs.

Steam emittance data are usually obtained from Hottel emittance charts [8,9], from emittance charts compiled by Ludwig, et al. [11], or from the Edwards exponential wide-band (EWB) correlations [12]. This latter model is based upon statistical models of gas absorption data in discrete wavelength bands. Nearly all the emittance data available have been obtained for gas pressures near atmospheric and in test chambers such that only moderate radiation path lengths (usually less than 1. m) were considered.

Utilization of the emittance charts requires extensive storage and a large number of source lines, both of which are prohibitive for the algorithm. Similarly, the exponential wide-band model formulation has a large number of source lines. Further, it is computationally time-consuming since band results must be computed in order to obtain the mean emittance. Therefore, the EWB model

is also not appropriate for HYBER. Instead, an emittance model based on a correlation of gas emittance data was selected. This correlation was developed by Cess and Lian for steam and air mixtures [13]. In this model, the Hottel emittance data have been fit to the exponential form shown below:

$$\epsilon_{ij} = a_0[1 - \exp(-a_1\sqrt{X})], \tag{11}$$

where

$$X = P_s B_{ij}\left(\frac{300P_g}{T_g}\right)(1 - \epsilon_s[b - 1]) \tag{12}$$

and

$$b = 5\left(\frac{300}{T_g}\right)^{0.5} + 0.5 \tag{13}$$

and a_0 and a_1 are functions of temperature given below.

Table 1.
Parameters Used in Cess-Lian Emittance Correlation

T (K)	a_0 (1)	a_1 $(m^{-0.5}atm^{-1})$
300	0.683	1.17
600	0.674	1.32
900	0.700	1.27
1200	0.673	1.21
1500	0.624	1.15

Note that pressure broadening effects are included in this formulation through X. In addition, the Cess-Lian correlation reduces to the well-known square-root dependence for the limit of non-overlapping strong absorption lines. The temperature limits specified above coincide with the range of experimental data used in the Hottel charts and omit the emittance data extrapolated by Hottel for the higher temperatures.

The Cess-Lian correlation agrees well with the EWB model and the emittance charts for the range of experimental data. For elevated pressures, temperatures, and/or large beam lengths, however, gas emittances computed from these models can vary by 10-25%. At this time, it is not known which method is most accurate for containment applications, and thus the model which is easiest to implement and which requires the least computational time was selected.

As a final note, two other participating gas species, carbon monoxide and carbon dioxide, can be generated from core-concrete interactions resulting from degraded core accidents. They are not included in the present radiation model, since the definition of their radiative absorption/emission properties would require the use of the EWB model, which is computationally prohibitive. Thus, these constituents are not included as participating species in HYBER. If carbon monoxide and/or carbon dioxide are present, their effects can be approximated by increasing the steam mole fraction. This can increase condensation effects, which may be undesireable. It should also be noted that these gases have different absorbing/emitting band regions and also have some bands that overlap with the steam bands; thus, the summing of the participating gas species mole fractions is not correct. Rather, the user is advised to review references [8,9] for help in modifying the steam mole-fraction to account for other participating gas species.

Radiation Enclosure Model

The radiative exchange model in SOLVER assumes that the wall temperatures and the gas environment are fixed during each time step. The net energy transfer is computed for each surface in the enclosure (equipment are treated as enclosure surfaces even if they are located in the enclosure interior) to obtain the net radiative heat transfer. Prior to performing these calculations, the gas emittance and transmittance, obtained from Eq.(14) below, are computed using the Cess-Lian correlation.

$$\tau_{ij} = 1 - \epsilon_{ij}(T_g) \tag{14}$$

Other important parameters which are needed in these calculations include the surface emissivities and the configuration factors. The configuration factors, as defined by Eq.(15), are geometrical factors which are measures of a surface's ability to view itself and other surfaces [8]. Implicit in the definition of configuration factors in Eq.(15) is the assumption that the surfaces are gray and diffuse absorbers/emitters.

$$F_{i-j} = \frac{1}{A_i} \int_{A_i} \int_{A_j} \frac{\cos\theta_i \cos\theta_j}{\pi S^2} dA_i dA_j \tag{15}$$

The angles in the cosine terms are measured from the normal vector for each surface.

Configuration factor reciprocity relations and the restriction that the factors for a surface must sum to 1.0 are satisfied when providing input to DATGEN and will not be discussed further in this text. Additional information pertaining to configuration factors and their determination is provided in the HYBER users' manual. The reader can also review references [8,9] for tabulations and closed form solutions for configuration factors derived for special geometries.

The single equivalent band model formulation for gaseous and surface radiative exchange, as taken from reference [8], is

$$\sum_{i=1}^{N\,surfaces} \left(\frac{\delta_{ki}}{\epsilon_{w_i}} - F_{k-i}\frac{1-\epsilon_{w_i}}{\epsilon_{w_i}}\tau_{ki}\right) q_{rad_i} = \sum_{i=1}^{N\,surfaces} (\delta_{ki} - F_{k-i}\tau_{ki}) e_{bw_i} - F_{k-i}(1-\tau_{ki}) e_{bg}, \tag{16}$$

where δ_{ki} is the Kronecker delta.

Since the surface and gas temperatures are known, the above relation can be used to obtain N linear equations for N surfaces in terms of the unknown radiative heat fluxes. These equations are solved using a Gauss-Jordan routine, which can solve up to three coupled equations. Note that if the gas is transparent, then the second term of the right-hand side of Eq.(16) vanishes, yielding the coupled enclosure equations which are independent of the gas temperature.

3.3.2 Convective Heat Transfer Models

Convective heat transfer results from the relative velocities and temperature differences between the gas and the surfaces within the enclosure. Depending on whether the gas or surface temperature is greater, heat can flow to the gas or to the wall. Two kinds of convective heat transfer are modeled in SOLVER, forced convection and free convection. Forced convection results from inertially driven gas flow, such as that induced by combustion processes and/or fan flow. In the absence of inertial flows, free convection takes place, where the velocity of the gas near the wall is due to buoyant forces arising from the temperature difference between the wall and the gas.

The convective heat flux, q, is equal to the product of a convective heat transfer coefficient, h, and the temperature difference between the wall, T_w, and the gas, T_g, as shown in Eq. (17).

$$q = h(T_g - T_w) \tag{17}$$

Convective heat transfer coefficients are usually correlated in terms of the Nusselt number, Nu, with parameters such as the Rayleigh number, Ra, for free convection and the Reynolds number, Re, for forced convection.† The literature is rich with such correlations which are usually derived from measurements of steady-state heat transfer rates. These correlations are commonly used in engineering calculations and are also the basis for predicting convective heat transfer rates in SOLVER.

Forced Convection

Two types of average, forced convection heat transfer correlations are included in HYBER. Either can be selected for use in post-combustion heat transfer analyses. The first model consists of the widely accepted Reynolds number flat-plate correlations. These correlations are for steady-state heat transfer for uniform flow over a flat plate. Reynolds numbers greater than $3(10^5)$ indicate that turbulent boundary layer phenomena control the heat transfer. The average Nusselt number (from which the heat transfer coefficient is inferred) in this case is given by [14]

†Definitions of these and other dimensionless parameters used in this text are given in the Nomenclature.

$$Nu = 0.037 Re^{0.8} Pr^{0.6} \tag{18a}$$

For Reynolds numbers less than $3(10^5)$, laminar boundary layer phenomena control the heat transfer. The Nusselt number relation for laminar heat transfer is given by [15]

$$Nu = 0.332 Re^{0.5} Pr^{0.667} \tag{18b}$$

These correlations are based on heat transfer coefficients measured on flat plates in a steady, uniform free-stream which flows parallel to the plate. These correlations do not depend on the orientation of the plate with respect to gravity. The length scale in the dimensionless parameters is the length of the surface in the direction of the flow. Different surfaces can thus have different heat transfer coefficients if they have different lengths. Note that the gas properties in the dimensionless parameters are evaluated at the gas temperature. Thus, as the gas temperature changes, the Reynolds number changes even though the gas velocity remains constant. New Reynolds and Prandtl numbers are computed each time step for each surface. The updated Reynolds numbers are used to determine which correlation (laminar or turbulent) will be used for the forced convection heat transfer coefficient.

A second, lesser known model for forced convection heat transfer is also included. This correlation is given by Means and Ulrich [16] and is based on phenomena similar to that which occurs during combustion, i.e., swirling, turbulent and decaying gas velocities. The data base for the correlation was obtained by venting a high pressure gas reservoir into a closed cylinder and measuring the heat transfer rate following injection. Further description of the experiment is given in reference [16]. The data were correlated with a gas Fourier number, Fo, to simulate the decay of heat transfer rates and gas velocity. The correlation is given by

$$Nu = 0.284 Fo^{-0.739} \tag{19}$$

The length scale in this correlation is the diameter of the vessel. Each surface of the vessel therefore has the same heat transfer coefficient. This does not imply that the heat flux on each surface is the same, however, because the heat flux is proportional to the temperature difference, which can vary from surface to surface.

Natural Convection

Natural convection, also referred to as free convection in this text, is usually correlated with the Rayleigh number which is a dimensionless number indicative of buoyant-driven flows. Natural convection is laminar if $Ra < 10^9$, and if $Ra > 10^9$ turbulent free convection occurs. Correlations for laminar and turbulent natural convection are included in HYBER. Turbulent convective heat transfer is given by

$$Nu = 0.098 Ra^{0.33} (T_w/T_g)^{-0.14}. \tag{20a}$$

This correlation was developed by Siebers [17] and includes a correction for the effects of large temperature differences. Recent studies have indicated that without such a correction, many correlations for turbulent free convection are not accurate if the ratio of the absolute temperatures of the wall and gas is large (greater than 1.1) [17,18]. The heat transfer coefficient is independent of the characteristic length of the surface due to the 0.33 exponent on the Rayleigh number. This scaling has also been observed for free convection in enclosures which makes the correlation convenient for use in HYBER. Note that all gas properties are evaluated at the gas temperature.

The laminar natural convection model in HYBER is the Schmidt-Beckman [19] correlation given by

$$Nu = 0.52 Ra^{0.25}. \tag{20b}$$

The gas properties in this correlation are typically evaluated at the average of the surface and gas temperature. In HYBER, the properties are evaluated at the gas temperature for numerical expediency. This approximation is not expected to introduce significant errors.

Both of the natural convection correlations described above are applicable only for vertical surfaces, where the characteristic length is the distance from the lowest end of the surface to the highest. The laminar or turbulent model is used depending on the value of the Rayleigh number which is calculated for each time step for each surface.

3.3.3 Condensatio.. Models

Condensation on Surfaces

Condensation on an enclosure surface occurs generally if the surface temperature is less than the saturation temperature of steam. The condensation rate is predicted using the Chilton-Colburn analogy between heat and mass transfer [20]. The mass flux to the wall is

$$\dot{M}_{cond} = K_g A_w (P_{sb} - P_{si}), \tag{21}$$

where K_g is the mass transfer coefficient, P_{sb} is the partial pressure of steam in the bulk gas mixture and P_{si} is the saturation pressure at the temperature of the gas-liquid interface for a surface of area A_w. The mass transfer coefficient is given by the Chilton-Colburn analogy as

$$K_g = (\frac{h}{\rho_g C_{p_g}})(\frac{P_g}{R_g T_g P_{bm}})(\frac{Pr}{Sc})^{0.667}, \tag{22}$$

where Sc is the Schmidt number, a dimensionless parameter which scales heat and mass transfer. P_{bm} is the logarithmic mean steam partial pressure given by

$$P_{bm} = \frac{P_{si} - P_{sb}}{\log(P_{si}/P_{sb})}. \tag{23}$$

The heat flux to the wall as a result of condensation, $\dot{Q}_{cond}$, is modeled as

$$\dot{Q}_{cond} = \dot{M}_{cond}(h_{fg} + C_{p_g}[T_g - T_i]). \tag{24}$$

Equation (24) accounts for the latent heat of vaporization and the energy lost in cooling the super-heated steam to the gas-liquid interface temperature.

Two models are included in HYBER to determine the gas-liquid interface temperature and the insulating effect of the liquid layer on a surface. Either

can be selected for use in mass transfer analyses. The first model assumes quasi-steady heat transfer across the condensate layer. The Nusselt film analysis for condensation [21] is used to compute the heat flux across the film as a function of the gas-liquid interface temperature as given by

$$\dot{Q}_f = 0.943[\frac{\rho_l(\rho_l - \rho_s)k_l{}^3 g h_{fg}}{\mu_l L(T_g - T_i)}]^{0.25}(T_g - T_i). \tag{25}$$

The characteristic length in this equation is fixed at 0.3048 meters since the equation is not valid for large lengths. The interface temperature, T_i, is varied until the heat flux across the liquid layer is within 0.1 percent of the sum of the convective, condensation and radiative heat fluxes incident on the liquid layer (see Figure 2). This iterative method of determining the gas-liquid interface temperature often fails to converge if the steam mole-fraction is greater than about 0.25. In this case, or if the quasi-steady assumption for condensation heat transfer is not appropriate, the second condensation model can be used.

The second model is based on the assumption that the condensate film provides no insulation from incident heat fluxes. This assumption is implemented by assuming that the interface temperature is equal to the wall temperature,

$$T_i = T_w. \tag{26}$$

Since this model does not require any iteration, it executes much more rapidly than the first condensation model. Results predicted with both models differ by only 5 percent, indicating that the second model is more useful, in general.

Nucleate Condensation in the Gas

Condensation within the gas is also modeled if the environment becomes super-saturated, i.e., the partial pressure of steam is greater than the saturation pressure at the gas temperature. In this case, steam is assumed to condense until the environment reaches saturation by means of a shock-like process. This process is thus referred to as condensation shock in this report. The quantity of steam condensed is determined by first writing expressions for the saturated and supersaturated steam mole fractions, X'_s and X_s, respectively.

$$x_s = \frac{N_s}{N_s + N_a} \tag{27}$$

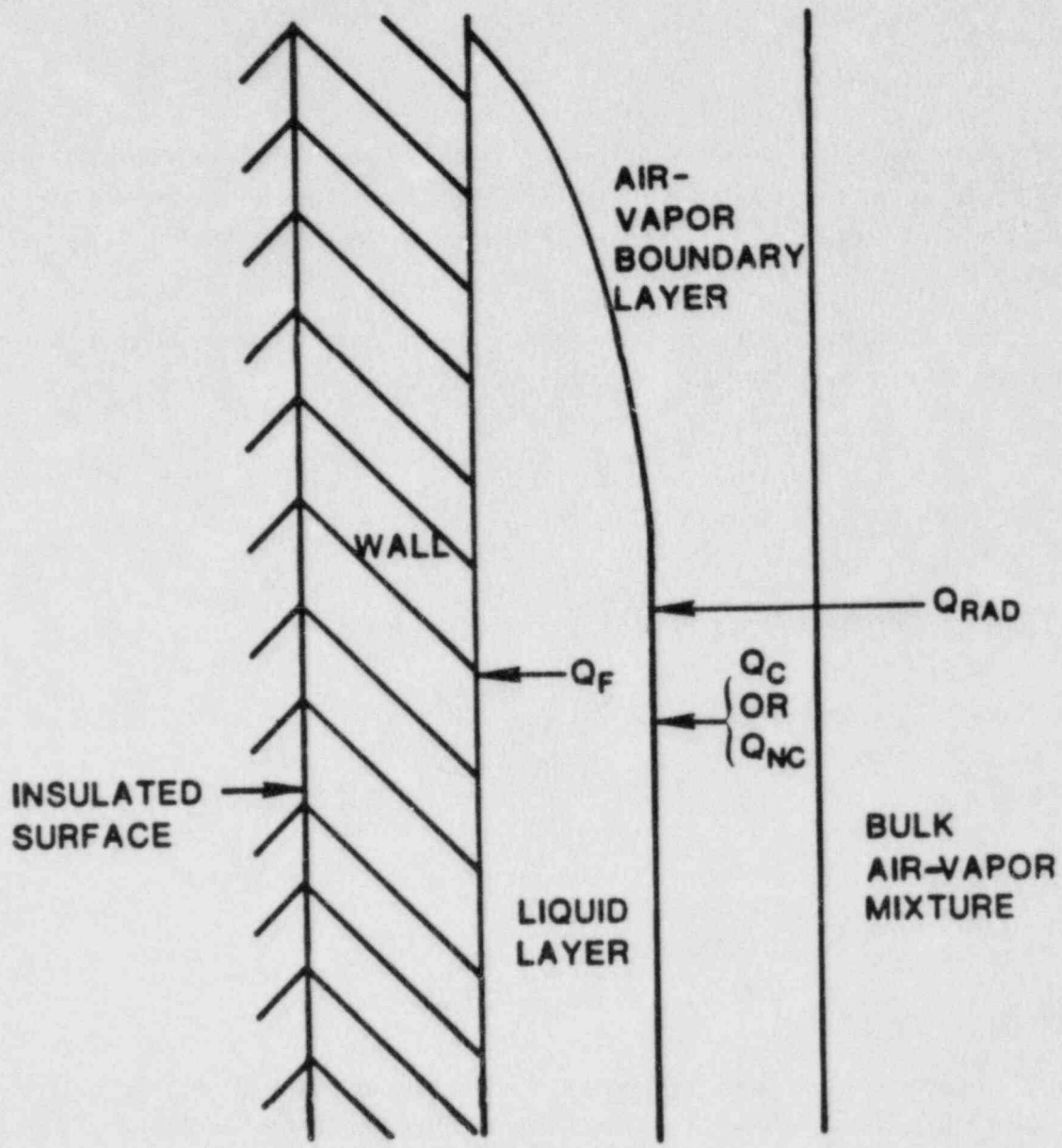

Figure 2. Schematic of heat transfer model for convection and condensation on a surface.

$$x'_s = \frac{N'_s}{N'_s + N_a} \tag{28}$$

where

$$x'_s = \frac{P_{sat}}{P_g} \tag{29}$$

N_a represents the number of moles of air (non-steam gas constituents) and N_s represents the moles of steam. P_{sat} is the saturation pressure at the gas temperature and P_{tot} is the total gas pressure. Variables with a "(')" represent quantities in the saturated state.

Since the moles of air do not change during condensation shock, the above equations can be solved for N_a and equated to yield

$$N'_s = \frac{N_s(1 - x_s)x'_s}{x_s(1 - x'_s)}. \tag{30}$$

The moles of steam that are to be condensed are given by

$$N_s - N'_s = \frac{N_s[1 - (1 - x_s)x'_s]}{x_s(1 - x'_s)}. \tag{31}$$

This decrease in the moles of steam results in a heat release to the gas given by

$$Q_{shock} = \overline{MW_s} h_{fg}(N_s - N'_s), \tag{32}$$

which increases the gas temperature and returns the gas to a saturated state. Once saturation conditions are reached, the gas state remains saturated and continuous nucleate condenation occurs for the remainder of the simulation.

3.4 Other Models

3.4.1 Water Spray Model

Water spray systems are designed to mitigate the effects of hydrogen deflagrations in nuclear reactor containments. As a water drop falls through the hot combustion gas, heat is transferred from the gas to the drop via coupled heat and mass transfer processes. The net result is that water is evaporated from the drop, steam is added to the gas mixture and, most importantly, the gas is cooled.

These phenomena are simulated for a field of falling droplets by considering a single water droplet of each size. For the purposes of modeling, one can consider a cylindrical volume which has a height equal to the total fall distance and a diameter equal to a certain sized drop diameter. Each droplet in this volume falls a short distance during a time step, but all the drops above and below it will also fall some distance during that time step. The sum of the fall distances for every droplet in this volume is then equal to the the fall height. This assumption allows an entire field of falling drops to be modeled as a single droplet of each size which falls the entire fall distance.

The water droplet evaporization model used in SO_4 ER includes an ordinary differential equation which describes the time rate of change of droplet mass [22]. This model has been modified for use in SOLVER by implementing the classical quasi-steady assumption that the droplet instantaneously reaches the saturation temperature. The effects of this assumption on the heat and mass transfer are discussed with the description of the model given below.

The time rate of change of the droplet mass is

$$\frac{dM_d}{dt} = -4\pi r^2 \rho_d \chi \mathcal{D}[\ln(1+B)], \tag{33}$$

where M_d is the mass of a drop of radius, r and density ρ .

The convective correction due to the distortion of the diffusive film is

$$\chi = 1 + .25 Re^{0.5} Sc^{0.333}. \tag{34}$$

The droplet Reynolds number is based on the drop diameter and a terminal velocity computed using the correlation given by Gunn and Kinzer [23],

$$v = [8/3gr\frac{\rho_l - \rho_g}{\rho_g C}]^{0.5}. \tag{35}$$

The droplet drag coefficient, C, is a function of the Reynolds number as given in the following correlation [24].

$$\begin{aligned} C \quad &= 27\ Re^{-0.84} \qquad && 0 < \mathrm{Re} < 80 \\ &= 0.271 Re^{0.217} && 80 < \mathrm{Re} < 10^4 \\ &= 2. && \mathrm{Re} > 10^4 \end{aligned}$$

The mass transfer parameter B is given by

$$B = C_{v_d}(T_g - T_{sat})/h_{fg}. \tag{36}$$

This equation shows that droplet mass loss occurs only when the gas temperature, T_g, is greater than the saturation temperature, T_{sat}. In order to calculate the mass evaporated, Eq.(33) is integrated over the user-specified fall distance each time step using a Runge-Kutta solver based on Gills' method. This solver was taken from reference [25].

The heat extracted from the gas during droplet evaporation is

$$Q_{spray} + G\Delta m[h_{fg} + C_{p_v}(T_g - T_d)], \tag{37}$$

where the first term accounts for the latent heat associated with the evaporated mass, Δm, and the second term is the energy required to heat the evaporated mass from the saturation temperature to the gas temperature. Both of these terms are multiplied by G, the flow rate for the specific drop size being considered.

The above heat and mass transfer calculations are performed separately for each drop size specified by the user. (Drop size data can be found from spray nozzle manufacturer literature.) The results are then summed to obtain the total heat and mass transfer due to the spray system. The heat and mass transfer rates are used only in the calculation of the gas state for the next time step, and do not directly effect the wall temperatures. That is, it is assumed that the sprays do not strike any walls of the containment or any of the equipment surfaces.

Note in Eq.(37) that the energy required to increase the droplet temperature to saturation temperature is not included. Computing the droplet heat-up would require the solution of an additional ordinary differential equation. This would substantially increase the execution time required for the spray model. Neglecting this sensible heat also tends to compensate for over-predictions of evaporation rates that arise from the quasi-steady assumption implicit in the ordinary differential equation described above.

Another important effect of the quasi-steady assumption is that the sprays have no effect after the combustion gas becomes saturated. For instance, if a large amount of steam is present and the atmosphere becomes saturated at 350 K, no heat or mass transfer between the gas and the sprays is modeled even if the spray temperature is below 350 K. In general, this has little impact on equipment survival analyses since saturation usually occurs at temperatures so low that the thermal effects on equipment are negligible.

3.4.2 Leak Model

Cracks or leaks in enclosure walls can have a significant effect on combustion phenomena by providing a means of pressure relief. The leakage rate is modeled as a quasi-steady mass flux through a user-specified leakage area. The exit velocity of the gas can be either sonic (choked flow) or subsonic. If the ratio of the confined pressure and the user-specified exit pressure indicates that the flow is choked, the gas velocity is calculated using confined gas conditions in the following equation:

$$v_e = \sqrt{\gamma R_g T_g}, \tag{38}$$

where γ is the isentropic index. For the choked case, the exit density is given in terms of the confined gas density by

$$\rho_e = 0.633\rho_g. \tag{39}$$

Flows determined to be subsonic from the pressure ratio evaluation are modeled using the steady state Bernoulli equation [25] with an orifice coefficient of 0.7. The exit velocity of the gas is

$$v_e = \sqrt{1.4(P_g/\rho_g - P_e/\rho_e)}. \tag{40}$$

The gas velocity in the enclosure is assumed to be zero and the density of the exiting gas is assumed to be the same as the enclosure gas density. The density at the exit plane is computed using the ideal gas equation of state with the user-specified exit pressure and temperature and the ideal gas constant for air. Note that flow is allowed into or out of the compartment depending on the compartment pressure and the user-specified exit pressure.

The mass leakage rate for either sonic or subsonic flow is

$$m_{leak} = \rho_e A_e v_e, \tag{41}$$

in which the exiting gas has the same composition as the compartment except during a combustion simulation, when hydrogen and carbon monoxide are not allowed to exit so that the user-specified combustion process can occur.

3.4.3 Model for Ice-Condenser PWR

Ice-condenser pressurized water reactors have a unique capability to mitigate the effects of hydrogen deflagrations. The containment primarily consists of a lower compartment and an upper compartment as shown in Figure 3. The lower compartment contains the reactor and a great deal of other equipment, whereas the upper compartment is a large, open volume. There are two flow passages between the compartments. The ice condensers are an annular passageway that extends approximately 300 degrees around the containment and contains baskets of ice. As gas flows from the lower compartment to the upper compartment, the ice cools and removes steam from the gas. One-way doors at the top of the ice condensers prevent flow from the upper compartment to the lower compartment through the ice condensers. Alternatively, upper compartment gases can flow to the lower compartment via a large set of fans in the center of the containment. A convective loop can be established in these reactors where lower compartment gas flows through the ice condensers as upper compartment gas flows into the lower compartment via the fans. During a hydrogen deflagration in the lower compartment, however, the hot gases can only expand through the ice condenser to reduce the peak gas pressure.

Even though SOLVER is designed to simulate only single compartment phenomena, the gas flows which are unique to ice-condenser PWRs can be modeled if simplifying assumptions are made. The first assumption is that all the steam is removed from gas flowing through the ice condenser. This results in only dry gas flowing into the upper compartment, which is therefore assumed to contain only a negligible amount of steam at any time. The upper compartment is also assumed to be adiabatic since the heat transfer, based on the previous assumptions, will be small. In order to maintain the validity of these last two assumptions concerning the upper compartment, a deflagration in the lower compartment cannot be simulated if the upper compartment water sprays are on or if a deflagration is occurring in the upper compartment. Additionally, flow through the fans is not allowed from the lower compartment to the upper compartment. These assumptions allow the inter-compartment flow to be simulated without tracking the upper compartment gas species, which are assumed to be the oxygen and nitrogen content of the pre-ignition gas.

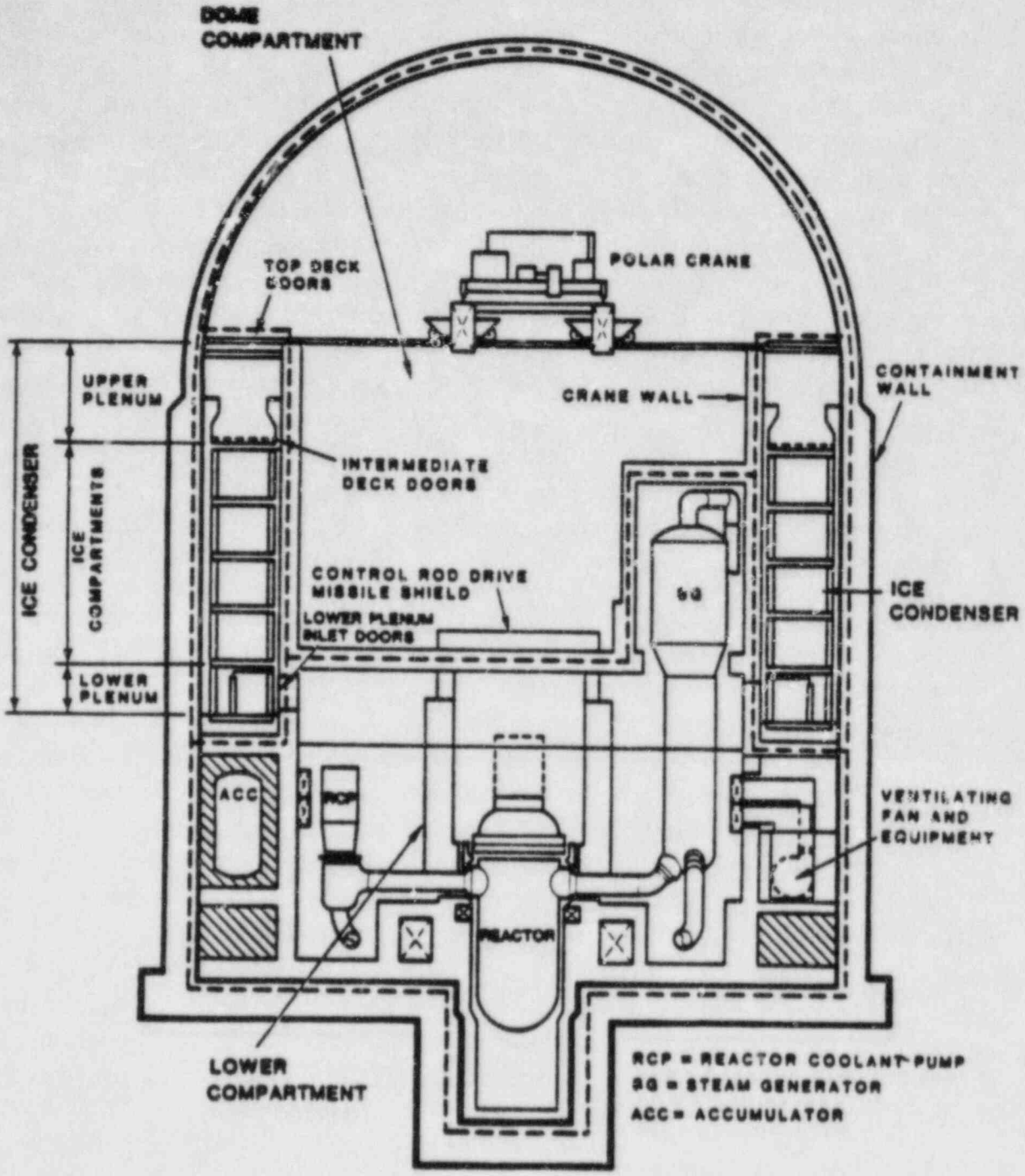

Figure 3. Schematic of an ice-condenser pressurized water reactor containment.

The gas flow through the fans and ice condenser are determined by the gas pressures in the two compartments. If the lower compartment pressure is greater, the gas flow through the ice condensers is modeled using the leak model described previously in Section 3.4.2. The inlet area of the ice condenser is user-specified and the gas density in the inlet plane of the ice condenser is the lower compartment gas density. The back pressure, or pressure at the ice-condenser inlet, is assumed to be the upper compartment pressure. Note that no flow is allowed through the fans in this case. If the pressure difference between the two compartments is within a user-specified tolerance, usually about 1 kPa, flow through both the ice condenser and the fans is modeled. The ice-condenser flow is modeled in the same manner described above and the flow through the fans is determined by comparing the fan flow rate and the flow rate that would occur due only to the pressure difference between the upper and lower compartment. The fan flow rate is given by the product of the upper compartment gas density and the user-specified fan rating. The pressure-induced flow rate is calculated using the leak model described above using a user-specified fan opening area. Note that this simple model is designed specifically for use in simulating deflagrations in the lower compartment of ice-condenser pressurized water reactors; its use for any other applications is not recommended.

3.4.4 Slab Conduction Model

Equipment and enclosure walls are modeled as slabs in SOLVER using a one-dimensional, planar conduction model. The transient conduction equation for each slab is given below.

$$\rho_w C_w \frac{\partial T}{\partial t} = k_w \frac{\partial^2 T}{\partial z^2} \tag{42}$$

subject to

$$-k_w \frac{\partial T}{\partial z}|_{z=0} = q_{net} \tag{43}$$

$$-k_w \frac{\partial T}{\partial z}|_{z=W} = 0 \tag{44}$$

and

$$T(z, t = 0) = User - prescribed \tag{45}$$

The material properties of thermal conductivity, density and specific heat are assumed to be constant, i.e., independent of temperature. As indicated in the boundary conditions, the front surface of the slab receives a net thermal input resulting from the previously described mechanisms of thermal radiation, convection, and condensation. The back surface is assumed to be adiabatic, i.e., perfectly insulated. This represents a conservative model for equipment since no conduction losses to mounting fixtures (i.e., heat sinks) are considered.

The above conduction equation is formulated using a Crank-Nicholson finite differencing scheme [26]. In this technique, the second order derivative is differenced in two equally weighted parts, one at the present time and one at the future time. This scheme is shown below for a node "i" positioned in the interior of the slab, assuming equal distance increments between the node one increment before (i-1) and one increment after (i+1).

$$\frac{k_w}{2}\left[\frac{T_{i+1}^{j}-2T_i^{j}+T_{i-1}^{j}}{\Delta z^2}+\frac{T_{i+1}^{j+1}-2T_i^{j+1}+T_{i-1}^{j+1}}{\Delta z^2}\right]=\rho_w C_w\frac{T_i^{j+1}-T_i^{j}}{\Delta t} \quad (46)$$

The "j" and "j+1" superscripts refer to the current and next time step, respectively.

This implicit formulation is unconditionally stable (but not unconditionally accurate), so that any time increment can be used. The equations generated for each nodal position are configured so that the total number of nodal coupled equations (n nodes) can be solved using a tridiagonal matrix solver, which is included in the algorithm.

Each slab can be modeled as a single material or as a composite of up to three different materials. When the single material slab option is specified, the user may divide the slab into two regions of different noding (coarsely and finely gridded sections) or may utilize a uniform grid. The former option allows the user to increase the spatial discretization near the front surface of the slab, where large thermal gradients would be expected during and immediately following combustion. In addition, a default option which divides the slab into two regions based on material property and total slab thickness is included. The criteria used in this meshing procedure was developed for HECTR [2] and resulted from a series of numerical experiments performed to optimize the grid size (i.e., limit the number of nodes) without sacrificing accuracy. When the slab consists of more than one material, noding must be uniform through each material but can vary from material to material. The thermophysical properties at the interfaces between materials are computed using nodal-length weighting as shown below.

$$\overline{\rho C}=\frac{\rho_i C_i \Delta z_i+\rho_j C_j \Delta z_j}{\Delta z_i+\Delta z_j} \quad (47)$$

$$\overline{k}=\frac{k_i \Delta z_i+k_j \Delta z_j}{\Delta z_i+\Delta z_j} \quad (48)$$

In the above expressions, the "i" and "j" subscripts refer to the thermophysical properties and nodal lengths for composite materials i and j, respectively.

The spatial discretization is formulated in DATGEN, where through interactive prompting, the user may change the slab mesh. The discretization is

fixed for a multiple burn sequence in the first data deck generation, when each slab is also initially assumed to be isothermal. When additional data decks are generated, the final previous slab temperature distribution will be saved and the previous noding must also be used.

3.4.5 Thermodynamic Model

Each of the models described above, with the exception of the wall conduction model, are used to determine heat and/or mass losses from the gas. The following section describes how these values are used to calculate new thermodynamic gas conditions each time step in the combustion vessel and, in the case of ice-condenser pressurized water reactors, in the upper compartment. Note that all calculations are performed under the assumption that the gas in the enclosure is at thermodynamic equilibrium.

Conservation equations for mass and energy are written for a control volume enclosing all the gas and liquid in the vessel, including the reservoir and sump used in spray systems. Throughout the analysis, no sensible heat transfer (i.e., non-phase change heat transfer) involving the liquid is considered. Therefore, conservation equations for the liquid are not required. This simplistic approach to the problem is appropriate for the scope of the HYBER calculations and is expected to yield useful equipment survivability predictions.

Conservation of mass for the gas is given by Eq.(49).

$$\frac{dM_g}{dt} = -\dot{M}_{cond} - \dot{M}_{leak} - \dot{M}_{ic} + \dot{M}_{fan} + \dot{M}_{evap} - \dot{M}_{shock} \qquad (49)$$

The first three terms are mass losses due to condensation on walls, mass leakage, and flow through the ice condenser. The following mass additions to the gas are fan flow from the upper compartment and steam addition from the evaporation of water sprays. The last term is the steam decrease due to condensation shock when the gas becomes saturated.

Conservation of internal energy for the gas is given by

$$\frac{d(MC_vT)_g}{dt} = -\dot{Q} - \dot{Q}_{spray} + \dot{Q}_{shock} + \dot{M}_{fan}h_u - (\dot{M}_{cond} + \dot{M}_{leak} + \dot{M}_{ic})h_g, \qquad (50)$$

where $\dot{Q}$ is the heat transferred to the wall by convective, radiative, and wall condensation heat transfer. $\dot{Q}_{spray}$ is the energy removed from the gas by evaporating water spray droplets, and the "h" terms are gas enthalpies. The mass and

energy equations can be combined, assuming ideal gas behavior, to obtain the time rate of change of the gas temperature.

$$\frac{dT_g}{dt} = [-\dot{Q} - \dot{Q}_{spray} + (\dot{M}_{cond} - \dot{M}_{evap})C_{v_g}T_g - R_gT_g(\dot{M}_{ic} + \dot{M}_{leak}) + M_{fan}(C_{p_u}T_u - C_{v_g}T_g) + \dot{M}_{shock}(h_{fg} + C_{v_g}T_g)]/(M_gC_{v_g}) \quad (51)$$

The new gas temperature, T'_g, is obtained from

$$T'_g = T_g + \frac{dT_g}{dt}\Delta t. \quad (52)$$

The new gas pressure is then obtained from the ideal gas equation of state

$$P_g = \rho_g R_g T_g, \quad (53)$$

where ρ_g includes the mass additions and subtractions which occurred in that time step.

For lower compartment, ice-condenser PWR analyses, the transient pressure and temperature of the upper compartment gas are also computed. An analysis similar to that shown above is performed, subject to the simplifying assumptions given in Section 3.4.3, yielding equations for conservation of mass and energy:

$$\frac{dM_u}{dt} = (1 - x_s)\dot{M}_{ic} - \dot{M}_{fan} \quad (54)$$

$$\frac{d(MC_vT)_u}{dt} = (1 - x_s)\dot{M}_{ic}h_{ic} - \dot{M}_{fan}h_u. \quad (55)$$

The terms containing x_s, the steam mass fraction of the lower compartment gas, result from the assumption that all the steam passing through the ice condensers is removed. The enthalpy of the dry gas exiting the ice condensers is h_{ic} , based on the user-specified exit temperature, T_{ic}. These equations can be combined to obtain the time rate of change of the upper compartment gas temperature.

$$\frac{dT_u}{dt} = [(1 - x_s)\dot{M}_{ic}(C_{p_{ic}}T_{ic} - C_{v_u}T_u) - \dot{M}_{fan}R_uT_u]/(M_uC_{v_u}) \qquad (56)$$

The new gas temperature and pressure in the lower compartment are computed in the same manner as described above for the combustion region.

4 Model Assessment

A large number of assumptions are employed in HYBER to facilitate the modeling of hydrogen deflagrations in single compartments. In the following paragraphs, several of the more important concerns that could result in inaccurate predictions using the models in SOLVER are described. Some of these concerns are scale-related, and thus become important for reactor geometry modeling. Other problems would be encountered in geometries of any size. These possible problems are highlighted here rather than in the individual model sections, since many of the problems are common to several of the models. Note that these effects will depend upon the particular problem to be solved using the algorithm. It is important that users of the algorithm understand these assumptions and their implications on results.

The assumption that the gas is in a uniform thermodynamic state deviates from actual phenomena. Elimination of this assumption, however, would require solution of field equations, as described in Section 2.1, which is not feasible. While the pressure is indeed spatially uniform, the gas temperature and composition in the enclosure can vary significantly. These non-uniformities are critical when estimating equipment thermal responses, because the heat/mass transfer is highly dependent on the local environment.

Application of widely accepted convection correlations in large- and small-scale vessels might also be incorrect for several reasons. First, the heat transfer phenomena during and immediately after combustion are highly transient. The use of steady-state heat transfer correlations in this situation will usually under-predict heat transfer rates. Second, the correlation parameters might not provide similitude for large-scale vessels such as reactor geometries. Similitude is expected for the range of parameters which occurred during the experiments from which the correlations are derived. These parameters include not only the dimensionless quantities such as the Rayleigh, Reynolds and Fourier numbers but also the characteristic lengths and gas/wall temperature ratios. Reactor containment length-scales and gas/wall temperature ratios often exceed those of the experimental data base. Thus, using these correlations constitutes an extrapolation of the data. Third, the correlations do not model all possible gas flow phenomena. Specifically, mixed-mode (forced/free) and transition-flow convective heat transfer are not modeled. In addition, the steady, uniform flow modeled in the Reynolds number correlations will probably never occur in a hydrogen deflagration.

Since mass transfer rates are obtained by the Chilton-Colburn analogy, the mass transfer model is subject to the same criticisms described above for the convection correlations. In addition, condensation can occur in a film-wise or drop-wise mode, but only a steady film model, which does not include the effects of non-condensible gases, is used in HYBER. This is mentioned even though mass transfer and condensation effects might not have a significant effect on the containment, because they might be important in predicting the response of safety-related equipment.

Similar criticisms can be directed towards the radiation model. Specifically, the gas is assumed to be gray when, in fact, strong spectral behavior is exhibited by steam. That is, the integration of peak spectral fluxes can differ from the peak flux computed for a single equivalent band. The single band gas emittance used in HYBER is obtained from the Cess-Lian correlation. This correlation agrees well with experimental data and predictive models such as the exponential wide band model for the data base. The data base, however, is not appropriate for pressure-beam lengths as great as those that occur in hydrogen deflagrations in large open volumes in nuclear reactor containments. The Cess-Lian correlation is valid only for steam-air mixtures and neglects thermal emission from other participating gases such as carbon monoxide and carbon dioxide which might be present during a degraded core accident. Similarly, this model is not for media which includes suspended particles such as water sprays or dust. Finally, such gas emittances are, strictly speaking, valid only for an isothermal gas contained by cold, black walls. This is probably not an accurate description of the reactor containment environment, especially for multiple burn scenarios.

The previous comments pertaining to the problems associated with scale are meant to emphasize the fact that results predicted using SOLVER for reactor applications might be inaccurate. This must be assumed because heat transfer data for reactor-sized length scales are not available. Thus, the use of "small-scale" correlations in reactor analyses can only be considered as "engineering approximations" until the data base is expanded. These concerns are also valid for other codes which use similar correlations. That is, the accuracy is questionable since the validity of the correlations used in reactor applications is not known. Since answers are needed now, however, the most appropriate correlations available have been implemented.

5 Computational Framework

The preceding two sections have described the function of each of the models used to represent various transport processes in HYBER and have pointed out possible shortcomings of these models. This section is intended to describe how all the models are integrated so that the user can better understand how the hydrogen deflagration scenarios are simulated. The discussion presented in this section will parallel the execution sequence shown in Figure 4. This section contains details of the calculational procedures performed in SOLVER and it is assumed that the reader has a general familiarity with the input requirements. For this information, the reader should refer to the algorithm users' manual [10].

The general execution procedure as shown in Figure 4 is as follows:

1. read in the information necessary to begin the problem,
2. compute the incident heat fluxes on the wall based on the present gas temperature and pressure, and wall temperature,
3. compute new wall temperatures based on the incident heat fluxes,
4. compute the heat and mass fluxes to the gas system that result from engineering systems,
5. determine the new gas state and new gas properties based on the summation of all the heat and mass fluxes,
6. return to step 2 to continue the calculation until the desired simulation time has been reached.

The purpose of the data initialization section is primarily to read in the geometric and thermophysical description of the enclosure, the configuration factors and beam lengths for use in thermal radiation calculations and the pre-ignition and adiabatic, isochoric combustion gas state. Additionally, the users' choice of models are read in this section. The data files used in this initialization section are generated in DATGEN, which is described in detail in the users' manual [10].

The first executable operation is to determine the initial state of the gas for the simulation. If heat and mass transfer are to be simulated during the combustion process, the pre-ignition conditions serve as the initial gas state.

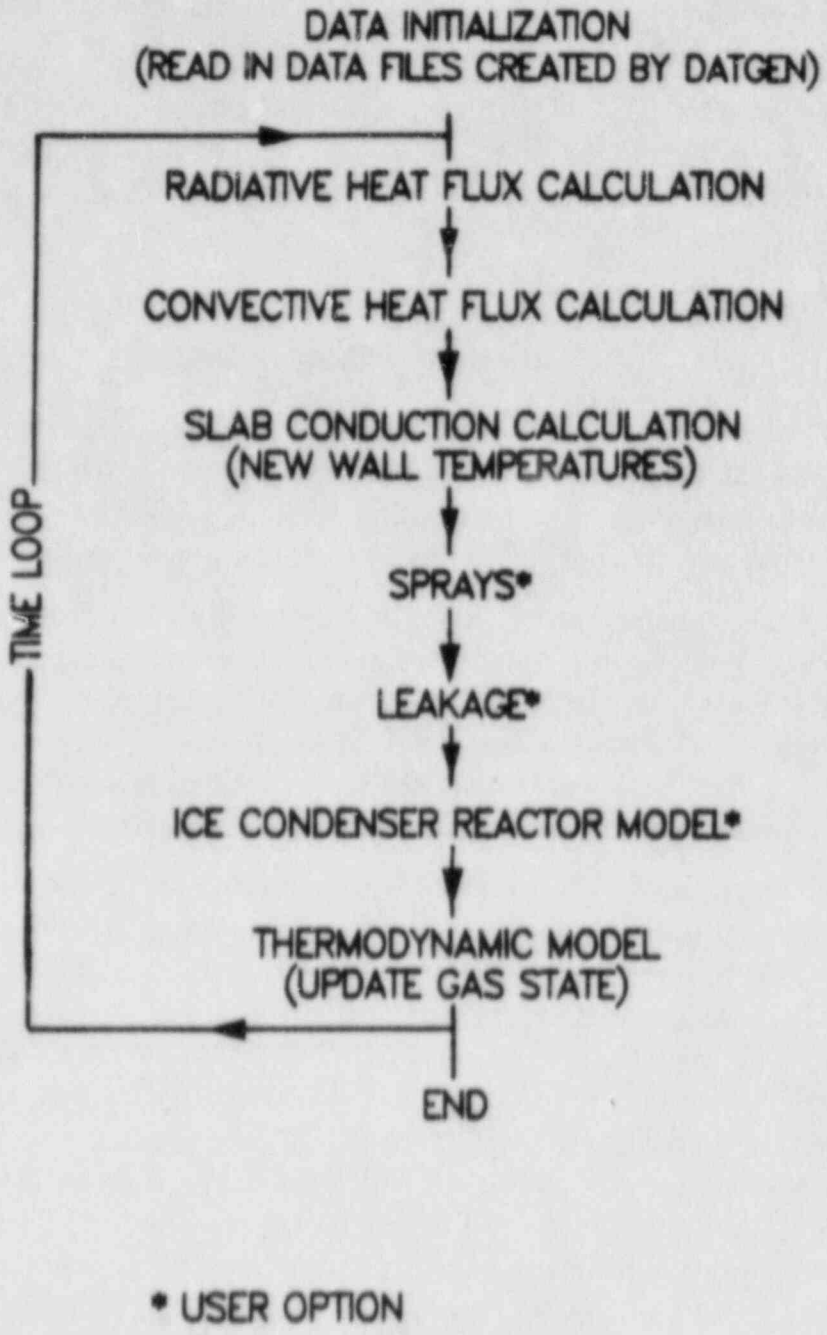

Figure 4. Execution path of SOLVER.

In this case, the Reynolds number convection correlations are used to predict forced convection heat transfer during combustion, based on the user-input burn velocity. If the combustion process is not to be simulated, the adiabatic, isochoric combustion gas state serves as the initial condition and the users' choice of forced correlations is implemented. Before exiting the initialization section, the initial gas properties based on the chosen initial gas state are computed.

Upon entering the time loop, the time-step control logic is encountered. As discussed in the users' manual, the time step is increased if the last gas temperature decrease is smaller than a user specified constant. This time step acceleration is given by

$$\Delta t = \Delta t_o + \Delta t_{in}, \tag{57}$$

where Δt_o is the present time step size, Δt_{in} is the original time step size chosen by the user, and Δt is the new time step size. This acceleration is not allowed during combustion simulations or on the first time step. The maximum time step allowed is a user-input. Maximum time steps should not exceed a few seconds.

The first heat transfer calculation is the solution of the radiative heat flux matrix (Eq.(16)). Wall or equipment surfaces that have surface temperatures below the saturation temperature, based on the steam partial pressure, are assumed to be covered with condensate. The emissivity of these surfaces is set equal to that of water, 0.94; otherwise, the user-specified emissivity is used. The solution of the matrix yields the radiative flux incident on each surface.

A calculational loop for each surface is required for convective and condensation heat transfer computations since the heat fluxes on each surface are usually different. In addition, the length scales in the Reynolds number and laminar Rayleigh number correlations can be different for different surfaces. (Recall that the turbulent free convection correlation is independent of length scale and that the Means-Ulrich correlation uses only the diameter of the vessel for a length scale.) Note that if the Means-Ulrich correlation is selected, it is not used until the combustion simulation is completed; at which time, the time variable in the gas Fourier number is set equal to zero. This simulates the post-combustion decay of gas velocity and forced convection heat transfer. Every time step, free and forced convection heat and mass transfer rates are computed in this section. The greater absolute (forced or free) value of the combined heat transfer rate associated with convection and mass transfer is used as the convective/condensation heat flux in further calculations for that time step.

At this point, the radiative, convective and condensation heat fluxes for each surface are added together to obtain the total, incident heat fluxes. These are

used in the conduction model to calculate the new temperature distributions in each slab. This completes the section of the code that predicts direct heat transfer effects on the enclosure surfaces. The remaining heat transfer calculations deal only with thermodynamic changes within the gas.

The effect of water spray evaporation on the gas environment is next considered. This model can be used either after or during and after a combustion process. The partial pressure of the steam must be greater than 0.06805 atm. for the sprays to be simulated. This is the lower bound of saturation pressure/saturation temperature data which are tabulated in the property evaluation routines. If the steam partial pressure is below this bound, an error message is written denoting the value of the steam partial pressure, and execution is terminated. As discussed above, the spray model does not simulate any water droplet evaporation when the gas environment is saturated. Since a post-combustion environment remains saturated once saturation is reached, the spray model is no longer used if saturation does occur.

The leak model and the ice-condenser PWR gas flow model follow as shown in Figure 4. An additional case is included in the latter model to allow for computational irregularities resulting from the quasi-steady flow assumption. This assumption implies that the upper compartment pressure is constant over a time step. If, however, the ice-condenser flow rate into the compartment is large, this assumption might be invalid. In such a case, the increase in upper compartment pressure due to the influx of ice-condenser gas can over-shoot the equilibrium pressure, resulting in an upper compartment pressure which is greater than the lower compartment pressure. In this situation, flow is allowed only through the fans, with the mass flux equal to the product of the upper compartment density and the fan rating. This will cause slight oscillations in the pressure to occur. They are usually small, and can be reduced by decreasing the user-specified time step or the minimum gas temperature change criteria used in the time step acceleration routines. More accurate simulations of the expansion process can be performed using codes such as HECTR or CLASIX which are designed to model multiple compartment nuclear containments.

The model for condensation shock follows next in the execution sequence. As explained in Section 3.3.2, this model simulates steam removal from a supersaturated environment by means of nucleate condensation in the gas. The test to determine if the environment is supersaturated occurs only if the gas temperature is below 505 K and the saturation pressure is greater than 0.06805 atm. The first limit is the upper bound of the tabulated heat of vaporization data used to calculate the energy addition in the gas. This limitation is not a great liability since the critical temperature for water, 640 K, would be the limit even if the

entire range of data were tabulated. The saturation pressure limit also results from bounds in the tabulated data.

The amount of steam removed by condensation shock is independent of sensible heat transfer processes which occur during each time step. Sensible heat transfer effects can result in a gas state (temperature and pressure) decrease such that the predicted steam removal rate yields a slightly superheated gas state. Thus, the gas state can oscillate slightly about the steam saturation line in modeling the condensation shock process. This variation is reduced by re-setting the time step to the initial, user-specified time step every time a supersaturated state occurs. This procedure yields oscillations that are not discernible on plots of the gas state.

The final calculation in the time loop is the determination of the new gas state for use in the next time step. The entire execution path descibed above is repeated until the user-specified simulation time is completed.

Upon completion of the time loop, all the information necessary to re-start the simulation is written to data files which are accessed by DATGEN. In addition, appropriate output data, e.g., surface temperatures, heat fluxes and gas state versus time, are stored throughout the simulation for use in equipment survival analyses. Details on the output formats are provided in the users' manual [10].

6 Comparison of Predictions with Experimental Data

Data from two hydrogen deflagration experiments are presented and compared with HYBER simulations in this section. This information is important for two reasons. First, these comparisons provide insights into the physical phenomena which occur during combustion processes. Such insights can be helpful to users when modeling hydrogen deflagration scenarios and aid in understanding the importance and use of critical input parameters associated with convective heat transfer such as gas velocities and characteristic lengths of surfaces. This information can also assist users in deciding which forced convection heat transfer model would be most appropriate for different applications. Second, the comparisons provide a basis for determining the accuracy of the heat transfer models (convection, condensation, radiation and conduction) in HYBER, which should enable users to realistically interpret calculations performed with the algorithm.

The combustion data presented in this section were obtained from experiments in the Fully Instrumented Test System (FITS) at SNLA and in the hydrogen dewar at the Nevada Test Site (NTS). The FITS facility is an "intermediate scale", cylindrical vessel, 5.6 m^3 in volume with 19.5 m^2 of surface area. The NTS dewar is a large, spherical vessel, 2084. m^3 in volume with 790. m^2 of surface area. Experiments are performed similarly in both vessels as follows: hydrogen is introduced into the vessel, creating a combustible mixture with air which is ignited with a spark plug or glow plug. The data recorded during and after a combustion process consist of gas pressure measurements. Additional data taken in the FITS test included the back-surface temperature of two brass flat-plate calorimeters which were 0.500 mm and 0.625 mm thick with surface areas of 0.023 m each. Unfortunately, similar calorimeters were not included in the NTS experiment analyzed.

Global (surface-area-averaged) heat fluxes, both total and radiative, are computed from the post-combustion pressure data using SMOKE, a combustion data reduction package developed at SNLA [27]. SMOKE is comprised of several computer codes which operate on the pressure data to provide estimates on the gas temperature and composition and the resultant energy transfer from the gas to the vessel walls. The gas composition at the completion of combustion is obtained from an AIC combustion calculation which utilizes the experimentally measured initial gas state and composition and the hydrogen combustion completeness. For later times, the gas is assumed to act as an ideal gas, and

the temperature can thus be directly related to the pressure. The gas temperature and the gas emittance, which is obtained using the Edwards exponential wide-band model [12], are used to compute the radiative heat transfer from the gas. The total energy transfer can be computed directly from the time rate of change of the pressure. The post-combustion steam mass loss through condensation is included, where applicable, using the extended Chilton-Colburn analogy [28] to relate the mass transfer and convective heat transfer coefficients. Since the gas composition is unknown during combustion, heat transfer results are only inferred for times after completion of combustion. SMOKE also includes an inverse conduction model which is used to compute local heat fluxes from the calorimeter temperature data. All of the computed heat fluxes are integrated to obtain energy depositions. For more information on SMOKE, see reference [27].

Two simulations were performed for each experiment to illustrate the differences between the forced convection models in HYBER. One simulation employs the Means-Ulrich correlation, and the other simulation uses the flat-plate, Reynolds number correlations, with a post-combustion gas speed of 1. m/s. This represents a spatially and temporally averaged, post-combustion gas speed for each experiment. Forced convection heat transfer during combustion is modeled using the Reynolds number correlations with the gas velocity equal to the flame speed, regardless of the post-combustion forced convection model chosen. Similarly, the same free convection model is used when either forced convection model is chosen. Thus, differences in post-combustion predictions in the following sections are due to differences in the forced convection models.

In each simulation, the specified flame speed was the vertical burn path length divided by the experimentally measured rise-time to peak pressure. The combustion completeness was adjusted until the peak predicted gas pressure matched the peak measured gas pressure. This procedure was necessary because combustion completeness data were not available. Given the completeness data, pre-ignition conditions, and the duration of the combustion process, the simulations could have been performed without such a matching process.

Prior to presenting the data and comparisons, it is necessary to define two terms that are used in the descriptions to follow. The term "global" refers to surface-area-averaged quantities and "local" refers to quantities that occur only in certain regions. For example, in the simulations of the FITS experiments, the vessel walls comprise nearly the entire surface area which exchanges heat with the combustion gases. Relatively little heat exchange occurs between the gas and the calorimeters since their surface areas are very small. Thus, the heat flux on the vessel walls multiplied by the vessel wall surface area is, for all practical purposes, the entire heat removal rate from the gas. This heat transfer dictates the gas pressure and temperature decay rates. Since the pressure is globally

uniform throughout the vessels in these problems (because flame speeds are small compared to sonic speed), the heat flux on the vessel wall is termed a "global" heat flux. Correspondingly, the heat flux on the calorimeters, which affects only the calorimeters and not the gas state, is called a "local" flux. Time-integrated heat fluxes, referred to as energy depositions below, are also termed "local" or "global" depending on the type of heat flux that was integrated.

In general, local heat fluxes are expected to be different from the global results since the gas temperature and velocity are non-uniform, resulting in local differences. For example, immediately following completion of combustion, the gas velocities and temperatures in the upper region of the vessel are expected to be greater due to buoyant forces and thermal stratification, respectively. In this case larger heat fluxes are expected in the upper region of the vessel than in lower regions where the gas is cooler. On the other hand, a flame propagating from the bottom of the tank to the top will result in larger heat fluxes in the lower region of the tank during the early portion of the deflagration. Since all calculations are based on the assumption that the gas environment is uniform in state and composition, these types of local effects cannot be resolved.

Local heat transfer effects are also due to differences in characteristic lengths of the calorimeters and vessel walls. These local effects can be resolved in HYBER, but are modeled differently by the two different forced convection models. The flat-plate, Reynolds number correlations depend on the characteristic length of each surface; thus the convective heat transfer coefficient is different for each surface if each has a different characteristic length. The Means-Ulrich correlation uses only the effective diameter of the vessel for a characteristic length, and thus the heat transfer coefficient is uniform throughout the vessel. The laminar natural convection correlation uses the characteristic lengths of each surface in all cases. On a related note, differences in beam lengths and configuration factors for the calorimeters and the vessel can result in local variations of radiative heat flux. This latter type of local effect is also modeled in the algorithm. Note that the location of each surface within the vessel is defined solely by the beam lengths and configuration factors between it and all other surfaces.

Predictions calculated using Means-Ulrich and Reynolds number convection models are compared directly with gas pressure, calorimeter temperature, heat flux, and energy deposition data in the following sections. From these comparisons, effects of the differences between the two forced convection correlations and the accuracy of the models on a local and global (i.e., average) basis can be evaluated. In addition, since the FITS and NTS vessels differ significantly in size, comparison of the FITS and NTS analyses illustrates the effects of length-scale on combustion phenomena and shows how different length-scales influence HYBER predictions.

6.1 FITS Data Comparison

The FITS hydrogen deflagration experiment chosen for this comparison was a ten percent hydrogen (by volume) test conducted on June 29, 1982. Particulars of the test are given in Table 2 below. Figure 5 is a schematic of the FITS facility. A Precise Sensor pressure transducer was used to measure the gas pressure and two flat-plate calorimeters were positioned in the FITS vessel as shown in Figure 5. These calorimeters have one-dimensional thermal response characteristics and are thus appropriate to be modeled in HYBER. A detailed description of the calorimeters can be found in reference [29]. The combustion burn length was 2.85 m, the rise-time to peak pressure was 1.1 seconds and the combustion was modeled as 92% complete. The ignition device was positioned in the lower region of the vessel; thus most flame propagation was in the upward direction. The FITS vessel walls were heated prior to ignition to prevent condensation on the walls. In the HYBER simulations of this test, three surfaces were modeled. Information on these surfaces are given in Table 3.

6.1.1 Comparison of Pressure and Global Heat Transfer

The transient gas pressure for the 10% hydrogen (by volume) deflagration in the FITS vessel is shown in Figure 6. The pressure rise to maximum pressure is nearly linear due to the short duration of the combustion process and the short burn length. The pressure rise appears to be well-modeled with the above specified flame speed and combustion completeness. The simulations of the post-combustion pressure decay also appear to be well-modeled although small deviations from the data are evident. The simulation using the Means-Ulrich correlation shows the pressure decay to be more rapid during the first six seconds after peak pressure, but slower after that time. The Reynolds number, flat-plate simulation, on the other hand, under-predicts the pressure decay throughout the experiment.

The difference in the gas pressures result from different global heat fluxes as shown in Figure 7. Only post-combustion heat fluxes are shown for the heat fluxes inferred from the pressure data (using SMOKE), since the technique to compute heat flux from pressure is valid only for the post-combustion data. The initial heat fluxes predicted using the Means-Ulrich, forced convection correlation far exceed the heat flux inferred from the pressure data, resulting in the initial, rapid pressure drop seen in Figure 6. At approximately 2.5 seconds, the heat flux

Table 2.

Initial Conditions for FITS Experiment

Estimated initial hydrogen mole fraction	0.100
Estimated initial nitrogen mole fraction	0.711
Estimated initial oxygen mole fraction	0.189
Estimated initial steam mole fraction	0.0
Measured initial gas pressure	0.900 atm
Measured initial gas temperature	375.0 K
Estimated combustion completion percentage	92%

Table 3.

Data for HYBER Simulation of FITS Test

Surface #1 – FITS Vessel	
Steel surface area	19.46 m^2
Steel thickness	25.0 mm
Steel emissivity	0.8
Length scale used in Reynolds model	3.4 m
Length scale used in Means-Ulrich model	1.4 m
Surface #2 – Brass Flat-Plate Calorimeter #1	
Calorimeter surface area	0.023 m
Calorimeter thickness	0.508 mm
Calorimeter emissivity	0.95
Length scale used in Reynolds model	0.152 m
Surface #3 – Brass Flat-Plate Calorimeter #2	
Calorimeter surface area	0.023 m
Calorimeter thickness	0.635 mm
Calorimeter emissivity	0.95
Length scale used in Reynolds model	0.152 m

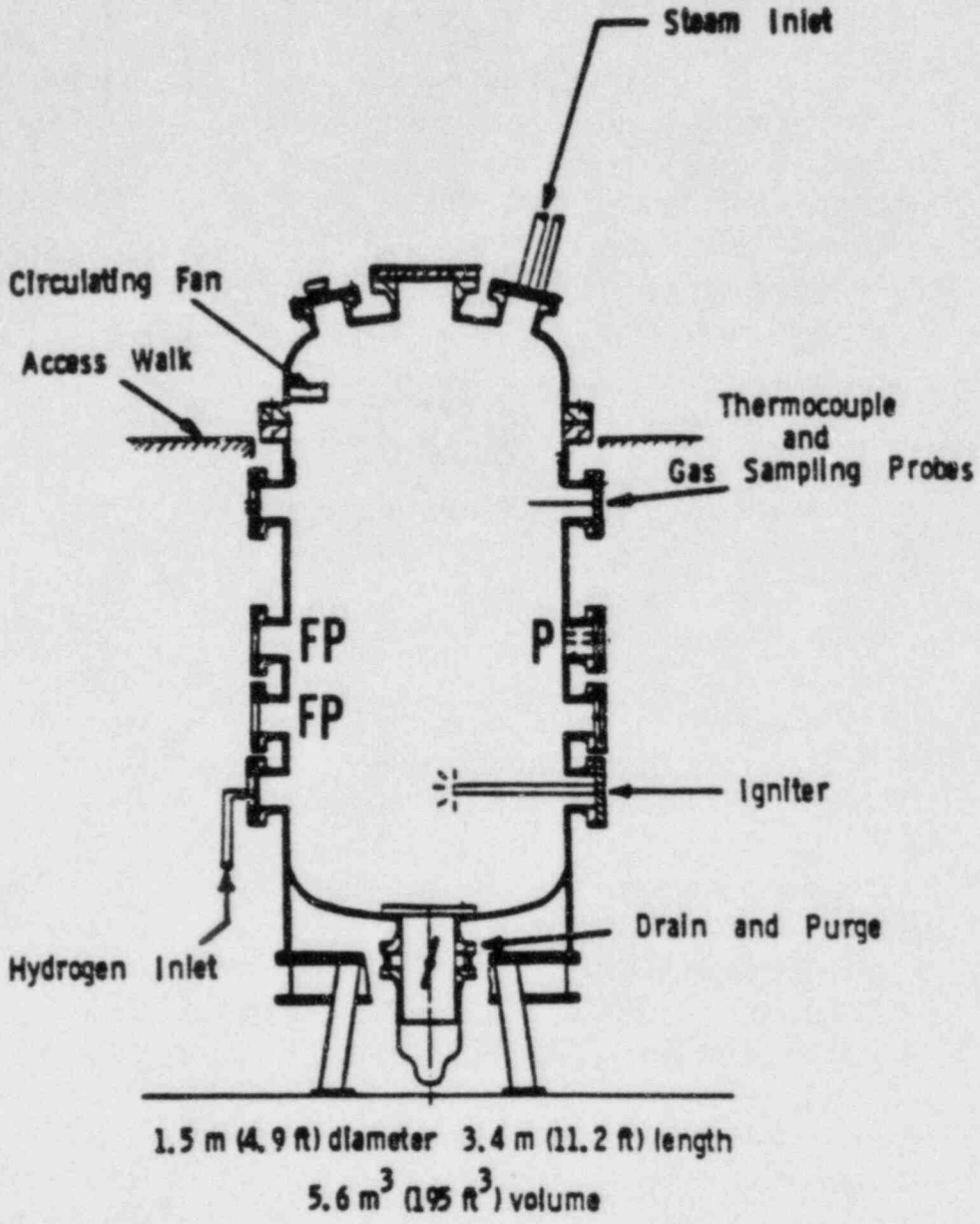

Figure 5. Fully Instrumented Test System (FITS).

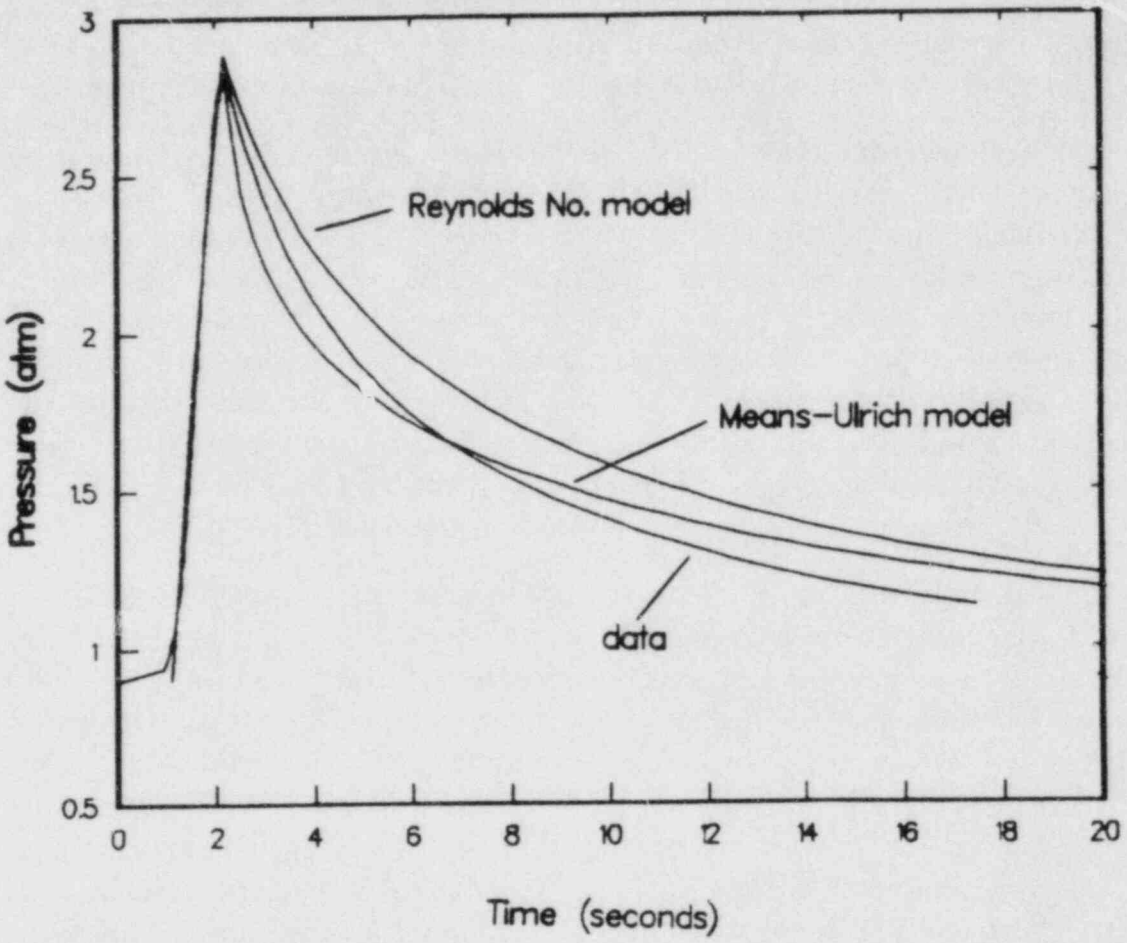

Figure 6. Gas pressure for the 10% hydrogen (by volume) deflagration in the FITS vessel (5.6 m^3).

predicted by the Means-Ulrich correlation is less than the natural convection heat flux predicted for the gas state and therefore the natural convection result is used. The natural convection heat flux is seen to under-predict the data after 3 seconds. Since the majority of data is for times greater than 3 seconds, the final pressure predicted by HYBER is greater than the measured pressure. Figure 7 also shows that the early predictions using the Reynolds number, flat-plate correlations are slightly lower than the pressure-inferred fluxes and under-predict them for the entire simulation. Thus, the pressure data are slightly lower than the predicted values. Figure 7 also shows that the convective heat transfer model used during the burn under-predicts the maximum measured (pressure-inferred) heat flux. This results because the Reynolds number, flat-plate correlation used in the combustion heat transfer model under-predicts convective heat transfer.

Figure 8 shows that the radiative heat fluxes computed in the simulation using the Reynolds number convection model are greater than the pressure-inferred radiative heat flux obtained using SMOKE. This is because the total heat flux was under-predicted, resulting in a greater gas temperature than in the experiment. Since the radiative flux is proportional to the gas temperature raised to the fourth power, the over-estimation of the gas temperature results in a greater radiative heat flux. Similarly, the radiative heat flux calculated in the Means-Ulrich simulation was relatively small because the over-predicted total heat flux resulted in a relatively low gas temperature, and hence a low radiative flux.

The most significant finding from the above comparisons is that heat fluxes are under-predicted several seconds after combustion. The under-prediction appears to occur as a result of forced convection heat fluxes decaying too rapidly and occurs for both simulations. At some point, computed natural convection heat fluxes are greater than the computed forced convection heat fluxes; thus HYBER uses the natural convection results in the calculations. The transition from forced to natural convection occurs earlier than the experimental data suggests. This apparent error is not surprising since the subject of transition regime convective heat transfer is not well understood. Figure 9 shows that despite this difficulty, the global energy deposition is modeled very well. The differences in the radiative energy depositions shown in Figure 10 are due to the reasons given in the preceding paragraph concerning radiative fluxes. This figure shows that radiative heat exchange accounts for approximately 50% of the total energy deposition.

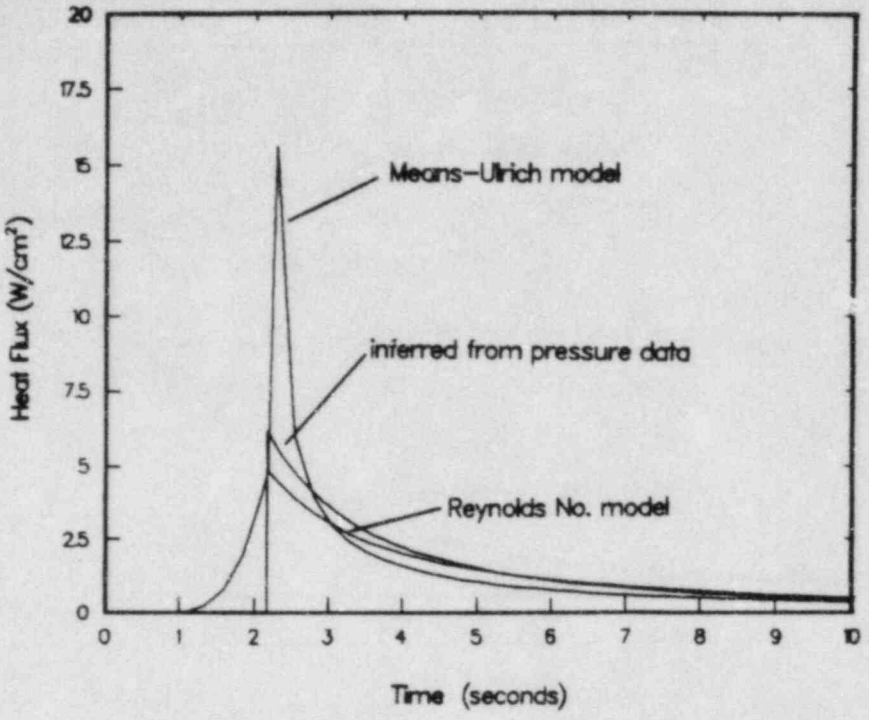

Figure 7. Global, total (convective and radiative) heat fluxes for the FITS experiment.

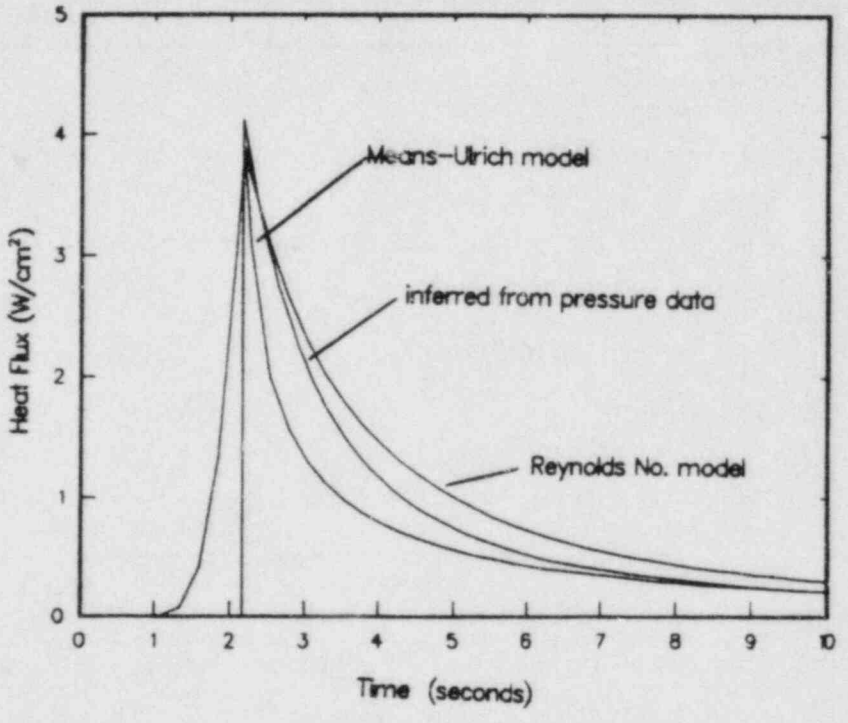

Figure 8. Global, radiative heat fluxes for the FITS experiment.

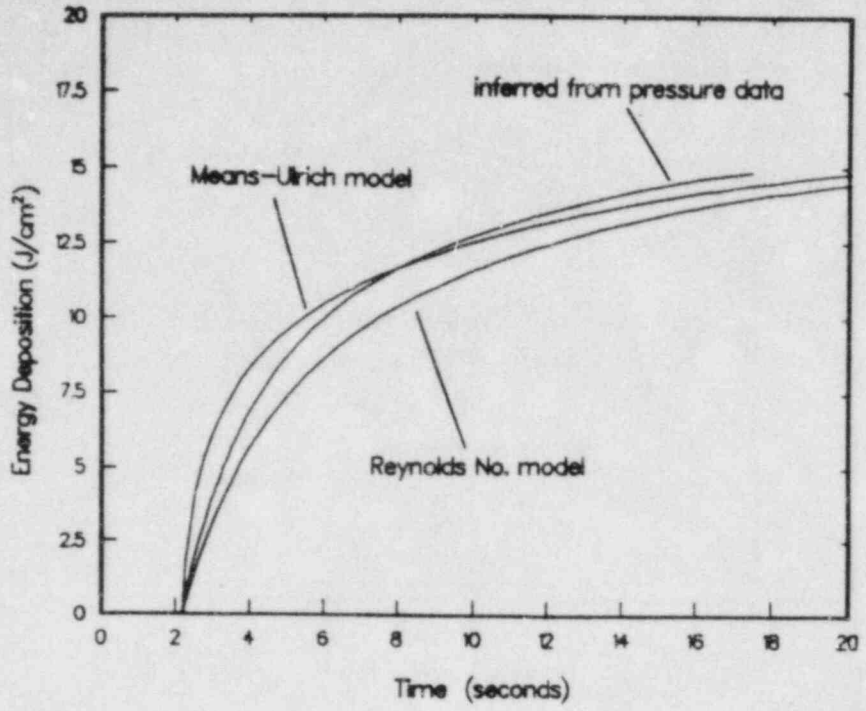

Figure 9. Integrated global, total heat fluxes for the FITS experiment.

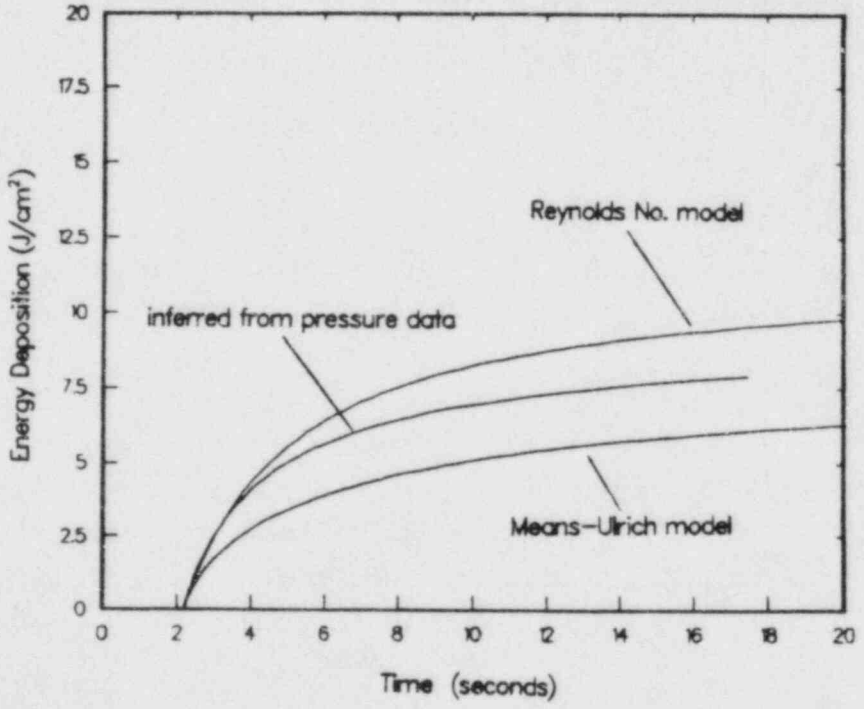

Figure 10. Integrated global, radiative heat fluxes for the FITS experiment.

6.1.2 Comparison of Calorimeter Temperatures and Local Heat Transfer

The data and predictions for the two flat plate calorimeters in the FITS experiment are shown in Figures 11 through 16. Flat plate #1 is 0.5 mm thick and was positioned on the FITS wall at approximately one half the vessel height. Flat plate #2 is 0.625 mm thick and was positioned slightly below flat plate #1.

The temperature data and results for simulations of flat plate #1 during the 10% hydrogen experiment in the FITS vessel are shown in Figure 11. The maximum temperature of the calorimeter is closely predicted by each simulation. The peak temperature predicted in the simulation using the Reynolds number convection model is slightly higher than the data and the prediction using the Means-Ulrich convection model is slightly lower. Note that both of the simulations predict the calorimeter temperature peaks to occur later than observed in the data. Also of interest is the rapid cooling exhibited in the data soon after the peak temperature occurred. The predicted cooling rates deviate from the data during this time period, but become very similar after about 60 seconds. That is, for late times, the temperature-time slopes are nearly the same.

Reasons for some of the trends in the calorimeter temperature data and predictions are evident in Figure 12, which shows the total heat fluxes obtained from the simulations and SMOKE. Notice that the heat flux data reached a maximum prior to the time at which peak pressure occurred (2.1 seconds from Figure 6). This time is assumed to be the time at which combustion is complete. Reaching a maximum flux before combustion is complete is an indication that the calorimeter was subject to locally high gas temperatures and velocities as the flame propagated towards the top of the vessel. That is, the peak gas temperature at the calorimeter location also probably occurred before completion of combustion, while the unburned gas above it remained at or near the pre-ignition temperature. This type of situation is not modeled in HYBER due to the uniform gas assumption. The predicted gas temperature in such a situation would be representative of an average of the burned and unburned gas temperatures. The predicted gas temperature would not reach a maximum until completion of combustion, and similarly, predicted maximum fluxes probably will not occur until completion of combustion, resulting in predicted peak temperatures which occur later than observed in the data. Figure 12 also shows that the convective heat transfer model used during combustion under-predicts the heat flux results obtained from SMOKE. The predictions could be improved by increasing the flame speed, but using flame speeds greater than those observed in experiments is not advised.

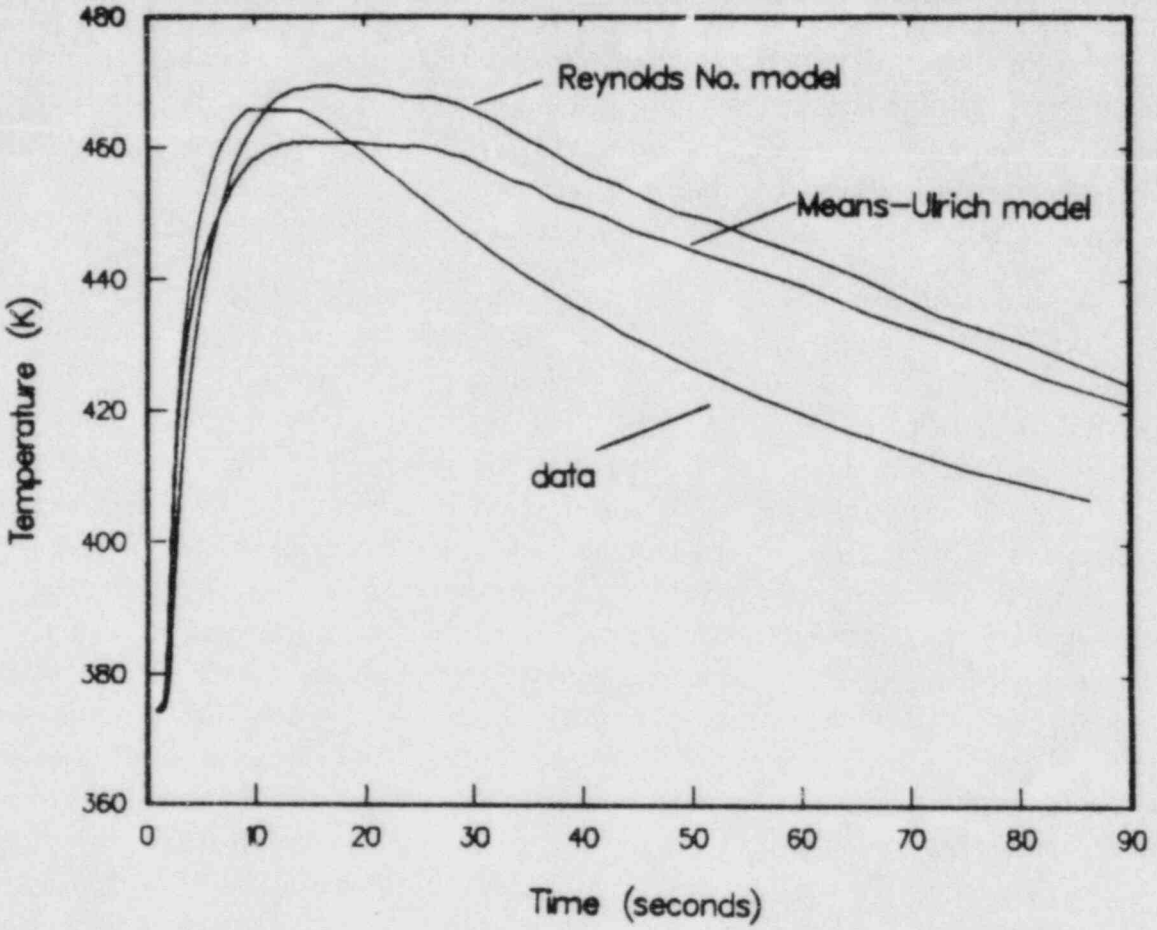

Figure 11. Thermal response of flat plate #1 in the FITS experiment.

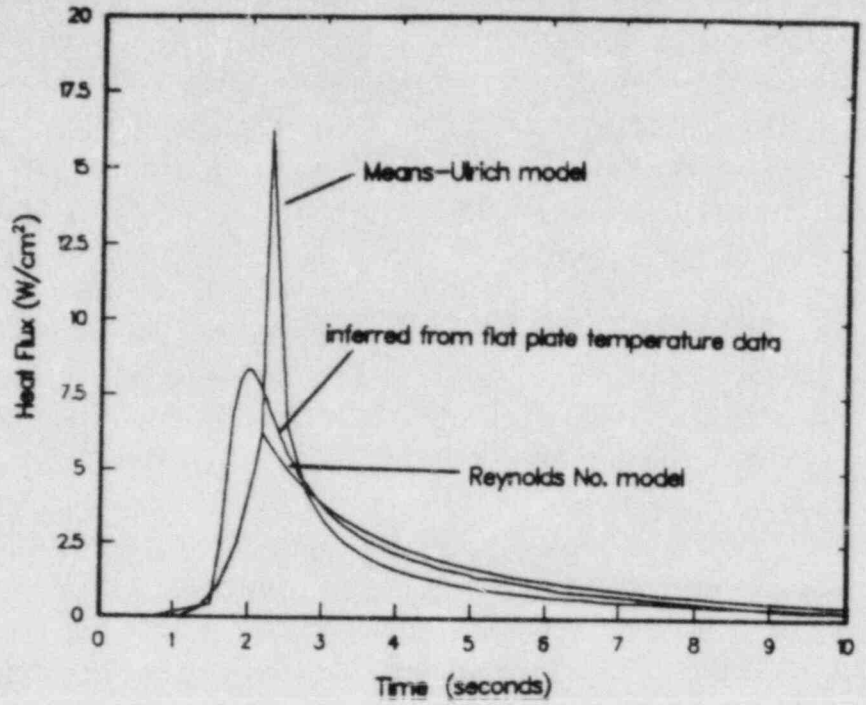

Figure 12. Local, total heat fluxes for flat plate #1 in the FITS experiment.

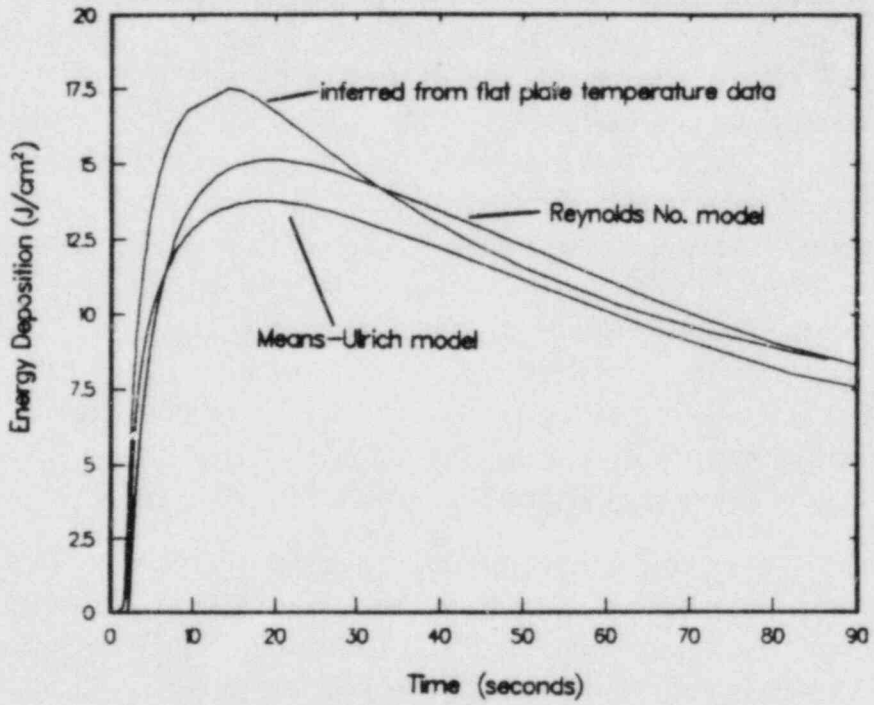

Figure 13. Integrated local, total heat fluxes for flat plate #1 in the FITS experiment.

The predicted levels of post-combustion heat fluxes also deviate from the data. The maximum flux computed in the simulation using the Means-Ulrich correlation is considerably greater than the maximum heat flux inferred from the calorimeter temperature data, but rapidly decays to natural convection heat flux levels. The simulation using the Reynolds number convective correlation under-predicts the heat flux throughout the simulation. These deviations in the heat flux results are seen to be of little consequence as shown in the integrated fluxes given in Figure 13. The large heat flux spike in the simulation using the Means-Ulrich model was of insufficient duration to have a significant effect other than to cool the gas to levels where the heat flux would be under-predicted. In general, the energy deposition results obtained from the calorimeter temperature data and the simulations agree quite well, the exceptions being the large energy deposition during combustion and the rapid cooling immediately after combustion. The large heating phenomena are attributed to local effects due to passage of the flame front near the calorimeter which, as previously explained, are not modeled in HYBER. Rapid cooling was also noticed in the comparison of the pressure and global heat fluxes and was attributed to difficulties associated with modeling transition regime convective heat transfer. This explanation is also applicable to the rapid cooling exhibited by the calorimeter data.

The temperature, heat flux, and energy deposition data and simulations for flat plate #2 are shown in Figures 14 through 16. The peak temperature and heat flux occurred before combustion was complete as with flat plate #1, but in this case, the simulations over-predicted the peak values. This probably is a local effect since flat plate #2 was in a lower position than flat plate #1. In this lower region, the gases probably were not as hot. The average gas temperature predicted in the algorthm was greater than the local gas temperature at the flat plate #2 location, resulting in over-predictions of the data. The rapid cooling following completion of combustion is not as distinctive as in previous cases. This is probably due to lower gas velocities in this region which resulted in transition regime effects being less important. Again, the convective heat transfer model used during combustion appears to be deficient, as seen in Figure 15, but it has only a small effect on the energy deposition shown in Figure 16.

Figure 17 shows the local and global heat flux data from the FITS experiment. Note that the heat flux inferred from the temperature data for flat plate #1 is greater than that of flat plate #2 and the pressure-inferred global heat flux. This information is provided to make the user aware that local effects cannot result in a wide range of results that can be predicted by HYBER. That is, global heat fluxes are less than local heat fluxes so that HYBER equipment thermal response predictions may not always be conservative.

In summary, the simulations of the FITS experiment have generally compared well with the data. The predicted gas pressures and calorimeter temperatures are within 10% of the data. Several discrepancies are evident and these should be kept in mind when performing simulations with the algorithm. Heat transfer during combustion and the cooling rates associated with the transition from forced to natural convection are, in general, under-predicted. Established free convection heat transfer appears to be well-modeled, however, as supported by the good agreement of energy deposition data. This is important since free convection is the dominant mode of convective heat transfer in most simulations. The agreement between HYBER simulations of calorimetry and the data would be expected to improve for more "thermally massive" objects. These trends have been observed previously in analyses performed on solid and hollow cubes included in tests conducted at the Variable Geometry Experimental System (VGES) [28].

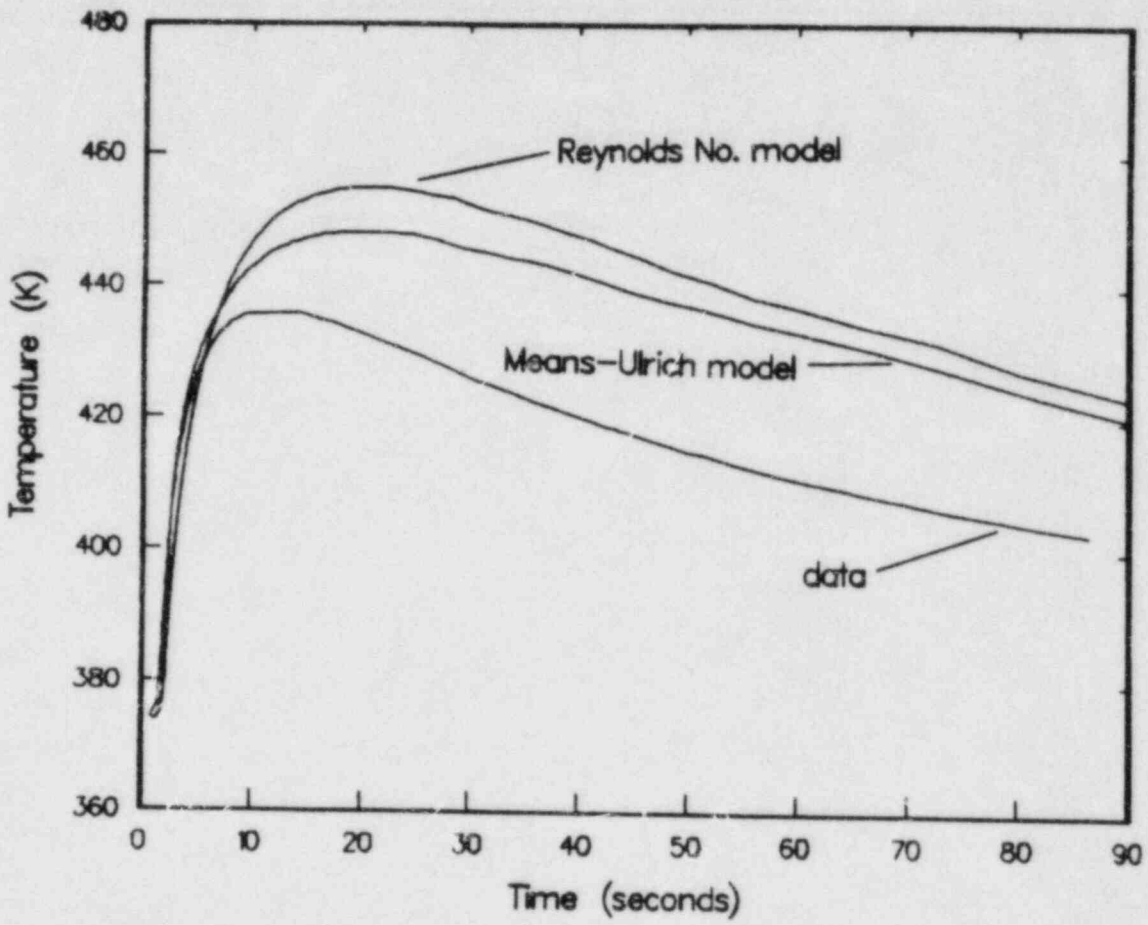

Figure 14. Thermal response of flat plate #2 in the FITS experiment.

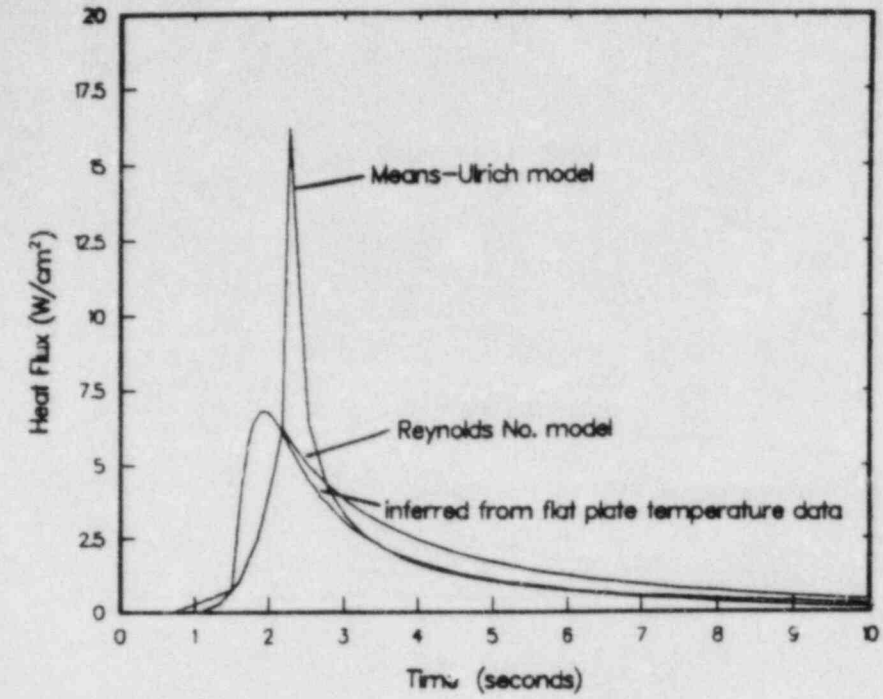

Figure 15. Local, total heat fluxes for flat plate #2 in the FITS experiment.

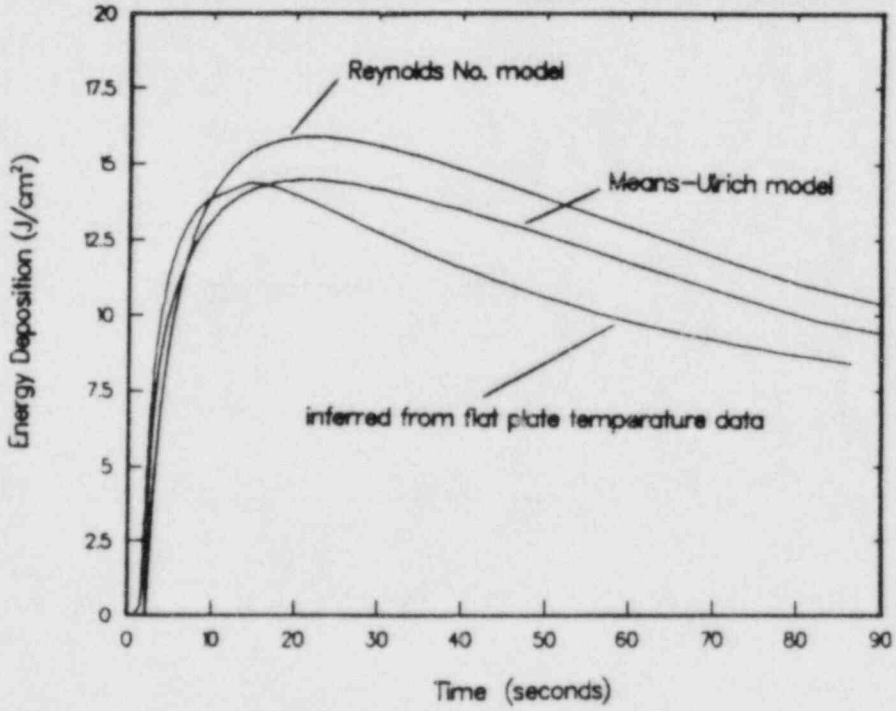

Figure 16. Integrated local, total heat fluxes for flat plate #2 in the FITS experiment.

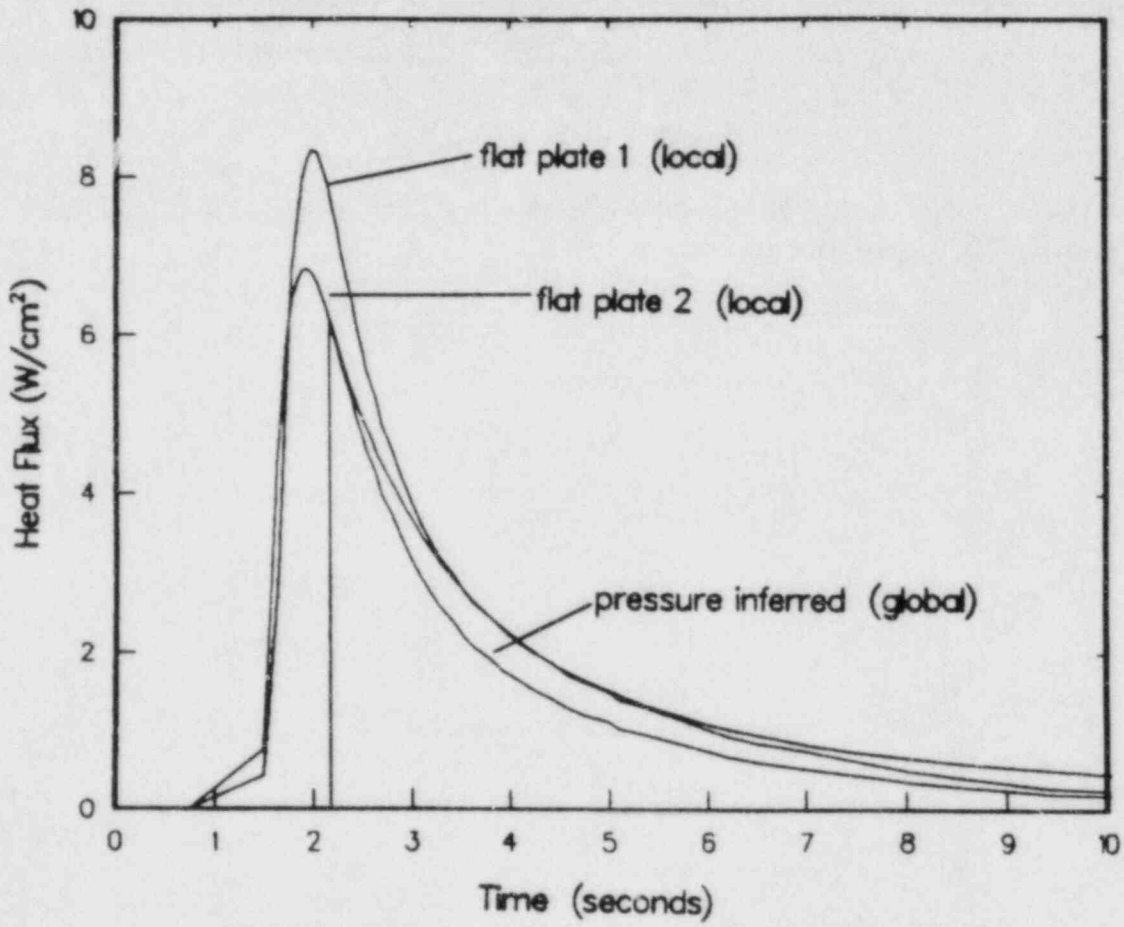

Figure 17. Comparisons of global and local total heat fluxes inferred from the FITS data using SMOKE.

6.2 NTS Data Comparison

The NTS experiment chosen for this comparison was a 6.3% (by volume) hydrogen deflagration conducted on July 28, 1983. The initial conditions for the experiment are given in Table 4. The burn length for the NTS vessel was modeled as 15. m, and the rise time to peak pressure was 14.5 seconds. The igniter was located near the bottom of the vessel, so that the flame propagation was, in general, in an upward direction. Note that no calorimetry data are presented for this test, thus only comparisons of global phenomena are made. Summary data describing the vessel and interior scaffolding as it was modeled using HYBER are given in Table 5.

Before presenting the data, the difference between the completeness of the 10% hydrogen deflagration in the FITS experiment (92%) and the 6.8% hydrogen deflagration experiment (52%) should be addressed. This difference is due to various combustion phenomena which occur for different initial hydrogen concentrations and could also depend on the length scale of the vessels. Well-defined methods to determine the completeness for a given deflagration are not available. As such, these types of problems lend themselves to parameter studies involving the burn completeness to bracket any results that could be obtained from algorithm simulations.

Table 4.

Initial Conditions for NTS Experiment

Estimated initial hydrogen mole fraction	0.068
Estimated initial nitrogen mole fraction	0.701
Estimated initial oxygen mole fraction	0.187
Estimated initial steam mole fraction	0.044
Measured initial gas pressure	0.925 atm
Measured initial gas temperature	303.1 K
Estimated combustion completion percentage	52%

Table 5.

Data for HYBER Simulation of NTS Test

Surface #1 – NTS Vessel	
Steel surface area	789.0 m
Steel thickness	25.0 mm
Steel emissivity	0.9
Length scale used in Reynolds model	15.0 m
Length scale used in Means-Ulrich model	15.85 m
Surface #2 – Scaffolding and Cat-walk	
Steel surface area	100. m^2
Steel thickness	6.25 mm
Steel emissivity	.9
Length scale used in Reynolds model	10. m

6.2.1 Comparison of Pressure and Global Heat Transfer

The gas pressure data and simulations for the NTS experiment are shown in Figure 18. The Means-Ulrich simulation predicts the pressure decay very well until about 40 seconds when it begins to predict higher pressures than were measured. The simulation using the Reynolds number convection correlation over-predicts the pressure throughout the simulation. Figure 19 shows that the total heat flux in this case was under-predicted which resulted in the higher than expected pressure. Again, only post-combustion heat fluxes obtained from SMOKE are shown for the data since the technique to compute heat flux from pressure is valid only for the post-combustion data. Figure 19 shows that the Means-Ulrich simulation provided the better heat flux estimates immediately after the combustion was complete. For this case, the deviation from pressure-inferred peak heat flux was small and the rapid decay in the data was well-modeled. Overall, both simulations modeled the heat fluxes quite well after about 100 seconds (see Figure 19). The radiative heat fluxes shown in Figure 20 indicate that the radiative heat transfer model matches the radiative heat fluxes inferred from the data quite accurately.

Figure 21 shows that the deviations seen in the flux comparisons have little effect on the integrated results. The offset between the data and the simulations is due to the initial under-prediction of heat flux immediately after combustion (as also seen in the FITS comparisons). The radiative energy depositions in Figure 22 are another indication of the good agreement between the data and the radiation model. Further, this figure shows that radiative heat transfer comprises approximately 50% of the total energy deposition.

In summary, the NTS analysis shows that simulated heat exchange during combustion is under-predicted although the pressure predictions are within 10% of the data. The Means-Ulrich model simulates post-combustion forced convection fluxes very well, but predicts transition to natural convection prematurely, which results in under-predicting much of the pressure data. The Reynolds number model under-predicts the post-combustion forced convection and also predicts premature transition to natural convection. The under-prediction of the heat fluxes results in only small deviations from the pressure and energy deposition data. Finally, the radiative heat flux predictions compare well with the heat fluxes inferred from the data (using SMOKE).

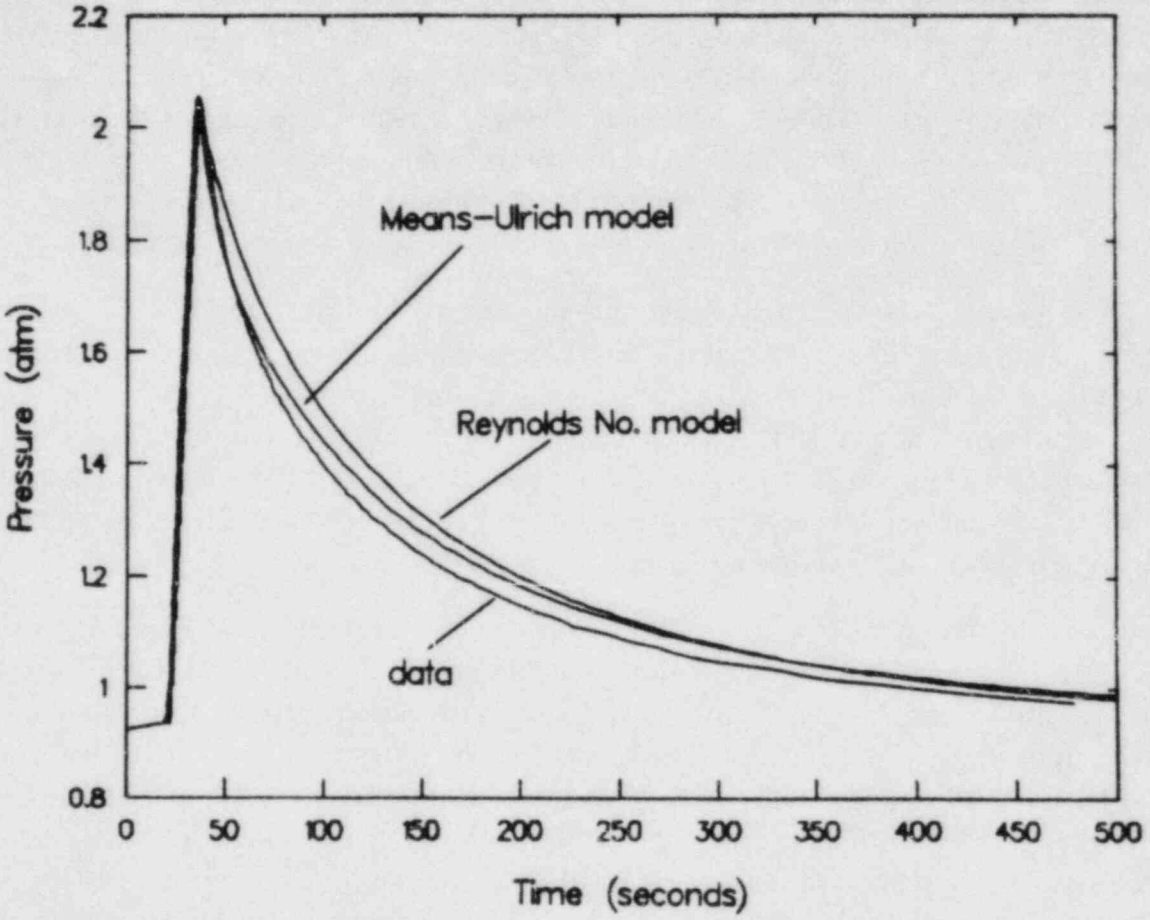

Figure 18. Gas pressure for the 6.8% hydrogen (by volume) deflagration in the NTS vessel (2084 m^3)

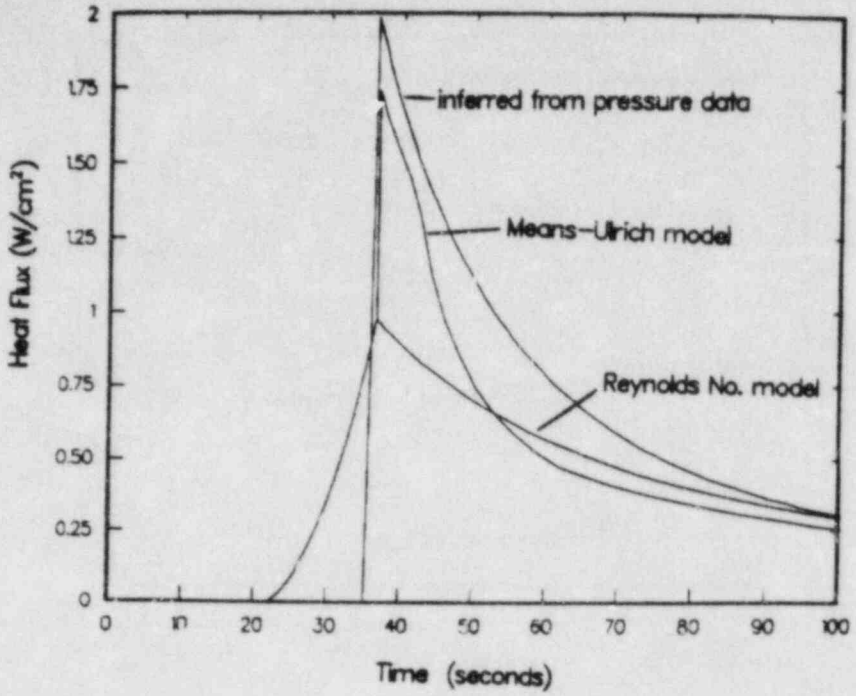

Figure 19. Global, total (convective and radiative) heat fluxes for the NTS experiment.

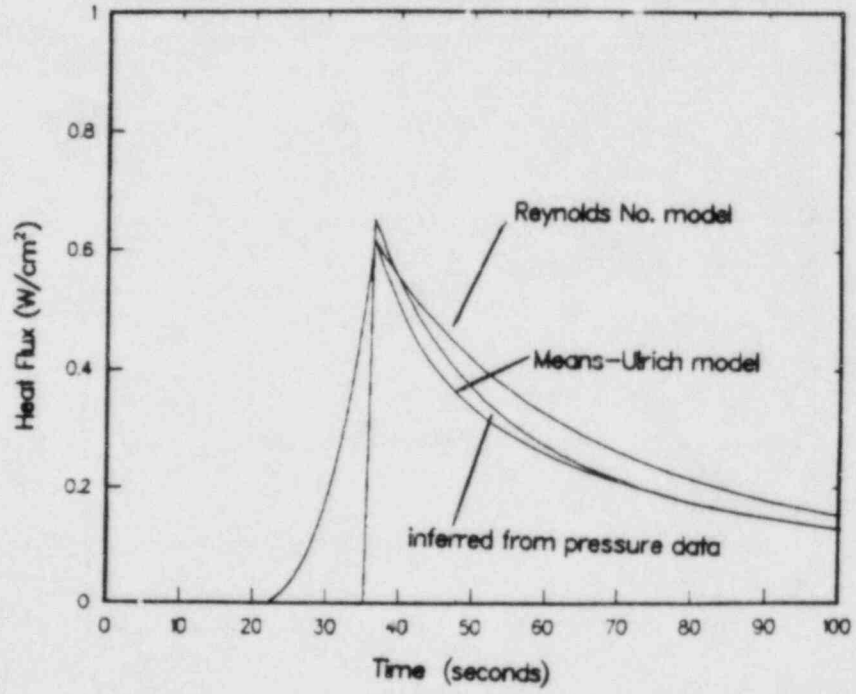

Figure 20. Global, radiative heat fluxes for the NTS experiment.

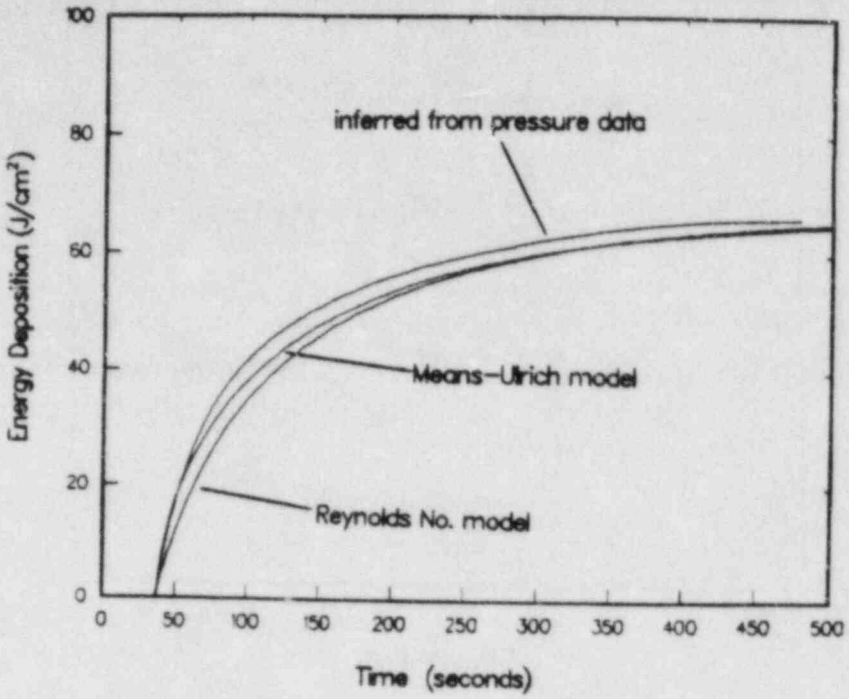

Figure 21. Integrated global, total heat fluxes for the NTS experiment.

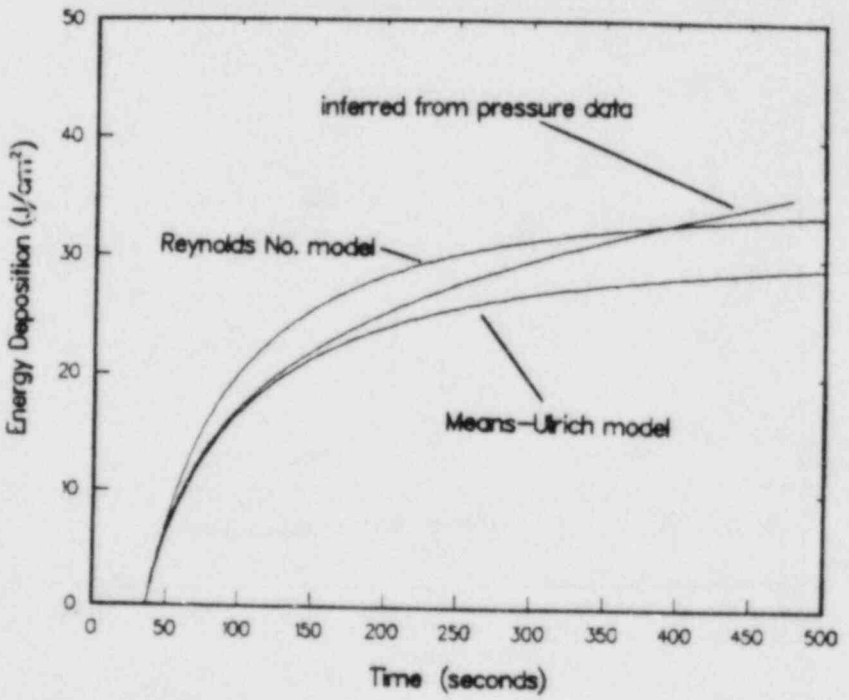

Figure 22. Integrated global, radiative heat fluxes for the NTS experiment.

6.3 Summary of Comparisons with Data and Recomendations

The magnitude of the differences between the simulations and the data have been avoided intentionally in the previous discussions. This is a recognition of the fact that the FITS and NTS tests are complex experiments, with a large number of coupled physical processes occuring simultaneously. The data do not represent precise measurements of well-controlled variables. measurements. In any experiment, there are errors in data measurements, but in global experiments such as these, comparing absolute values to a high level of precision is not warranted. It is believed that the data analyzed in these studies are representative of data taken in most combustion experiments. The comparisons are intended to show that trends seen in the data are also predicted in HYBER and to show that the general relationship between the simulations and the data is reasonable.

The following trends have been noted from the two comparisons performed. In each experiment, combustion heat fluxes were under-predicted. For post-combustion convective heat transfer, the Means-Ulrich forced convection model predicted peak heat fluxes more accurately than the Reynolds number model. The fact that the Means-Ulrich model over-predicted the peak flux in the FITS simulation and slightly under-predicted the peak flux in the NTS experiment is probably a result of length scale effects. The Reynolds number model under-predicted the peak flux for both tests, although different user-specified gas velocities could have been used to increase the heat fluxes predicted with this model. Both of the correlations under-predicted heat transfer several seconds after completion of combustion apparently as a result of modeling the onset of natural convection prior to the time when transition actually occurred. The effects of these deviations on the gas pressure and global energy deposition are nonetheless small. Typically, the simulations were within 0.1 atmosphere of the pressure data. The radiative heat fluxes also agreed well with the data.

The comparisons of the calorimetry data and predictions indicated that the same difficulty in modeling transition-regime convective heat transfer occurred on a local basis. The thermal environment affecting the two calorimeters differed from the global environment due to spatial variations in the gas state (density and temperature) and velocity that are not modeled in HYBER. As a result, the flat plate #1 simulation predicted the peak calorimeter temperature to within a few degrees and the flat plate #2 simulation under-predicted the peak temperature by a larger amount, but was still within 10% of the data. Therefore, users should be aware that a wide range of results can occur as a result of local effects. Generally, however, the simulations provided a good estimate of the thermal response of the calorimeters.

These comparisons indicate that the heat transfer models in HYBER provide reasonably accurate estimates of the overall heat exchange resulting from a hydrogen deflagration. The comparisons, however, also indicate that certain discrepancies can occur. The discrepancies in the comparisons made here are not large, but could become important in some problems. For example, the algorithm does not resolve local effects (e.g., position in tank, spatially varying gas state and velocity) that can be important in determining the response (burn survival) of individual safety components. The comparisons also indicate that the length scale of a vessel can effect the simulation of heat exchange between the gas and vessel. Thus, the ability of HYBER to model heat transfer in much larger-scale vessels is not known. The simulations of the FITS and NTS experiments are within 10% of the measured gas pressure and calorimeter temperature data. It is expected that the user can obtain a reasonable estimate for most problems by performing parameter studies to find limiting cases for a given combustion scenario. Parameters that can be easily varied are the gas velocity, the flame speed, the characteristic length of a surface (not the thickness), the diameter of the vessel, the emittance of any surface, the burn length, the combustion completeness, and the type of forced convection and condensation model used. The user should refer to the users' manual, reference [10], for information regarding how to modify data files to perform such parametric studies.

Finally, it is noteworthy that in both of the examples presented, the radiative heat transfer was found to be about 50% of the total energy loss from the gas. It has been postulated that convection heat transfer effects would become less important as the vessel size increased, and that for reactor-scale geometries, radiative energy transfer would be dominant [29,30]. These trends have been predicted based upon analyses which have used Reynolds number convection correlations which are a function of nuclear containment surface length scales. In these models, the larger the length scale, the smaller the Reynolds number predicted convection coefficient becomes. Results obtains in this study imply that reactor surface length-scales may be inappropriate, however, and smaller values may need to be used. Since such questions have not been resolved, these uncertainties should be considered in analyzing large-scale geometry problems. That is, parametric variations of the length scale should be considered when assessing the effects of convective heat transfer to/from large surfaces.

7 Summation

This report describes the phenomena associated with deflagration processes in single compartment confined vessels. The coupled heat and mass transport processes have been modeled by applying simplifying engineering assumptions which allow for solution of the problem. Using these approximations, an equipment survival algorithm, HYBER, consisting of two codes, SOLVER and DATGEN, has been developed. As prescribed in the initial charter of this work, the codes are small and self-contained and operate on personal computer systems. The heat and mass transfer models included in the algorithm are described in this report along with precautions about the applicability and limitations of those models.

Comparisons of predicted results with experimental data for the gas pressure and calorimeter thermal reponses obtained from intermediate- and large-scale combustion experiments have been provided. Overall, these comparisons are favorable, especially when appropriate correlations are selected. It must recognized, however, that using the algorithm to predict component thermal responses and environment conditions in nuclear reactor containments is an extrapolation beyond the range of experimental validation. Appropriate correlations have been included in HYBER, so that predictions of the consequences of deflagration processes in reactor containments should be qualitatively correct. Further, HYBER is expected to perform these computations at least as well as other computer codes presently available, so long as the geometry can be modeled as a single physical compartment.

HYBER was developed to provide scoping calculations of equipment thermal response for use in nuclear reactor equipment survival studies. It also provides quantitative predictions for the environment subject to the assumptions described in the report. In addition, HYBER can be used to model intermediate- and large-scale hydrogen–air combustion experiments. It is primarily intended, however, to serve as a tool which will support NRC licensing activities pertaining to equipment survival analyses.

(This page intentionally left blank)

References

1. The CLASIX Computer Program for the Analysis of Reactor Plant Containment Response to Hydrogen Release and Deflagration, *Offshore Power Systems*, OPS-367A31.

2. **Camp, A.L., Wester, M.J., Dingman, S.E., and M.P. Sherman**
HECTR: A Computer Program for Modelling the Response to Hydrogen Burns in Containment, *Proceedings of the Second International Conference on the Impact of Hydrogen on Water Reactor Safety*, Albuquerque, N.M., October 3-7, 1982.

3. **Wooton, R. O. and H. I. Avci**
MARCH (Meltdown Accident Response Characteristics) Code Description and Users Manual, *Battelle Columbus Laboratories*, BMI-2064, 1980.

4. JANAF Thermochemical Data *DOW Chemical Co., Thermal Research Laboratory*, Midland, Michigan.

5. **Reid, R. C., Prausnitz, J. M., and T. K. Sherwood**
The Properties of Gases and Liquids, McGraw-Hill Publishing Company, N.Y., 1977.

6. **Whitley, R. H.**
Condensation Heat Transfer in a Pressurized Water Reactor Following a Loss of Coolant Accident, PhD. Thesis, University of California at Los Angeles, 1976.

7. **Baer, M. R. and A. C. Ratzel**
A Hydrodynamic Model of Hydrogen Flame Propagation in Reactor Vessels, *Proceedings of the Second International Conference on the Impact of Hydrogen on Water Reactor Safety*, Albuquerque, N.M., October 3-7, 1982.

8. **Siegel, R. and J. R. Howell**
Thermal Radiation Heat Transfer, 2nd Edition, McGraw-Hill Publishing Company, N.Y., 1981.

9. **Hottel, H. C. and A. F. Sarofim**
Radiative Transfer, McGraw-Hill Publishing Company, N.Y., 1967.

10. **King, D. B., Ratzel, A. C., and S. N. Kempka**
Users Guide for HYBER, the Hydrogen Burn—Equipment Survival Algorithm, *Sandia National Laboratories, Albuquerque, N.M.*, SAND84-0160, 1985.

11. **Ludwig, C. B., et al**
Handbook of Infrared Radiation from Combustion Gases, *NASA Publication*, NASA SP-3080, 1973.

12. **Edwards, D. K.**
Molecular Gas Band Radiation, *Advances in Heat Transfer,* **12,** Academic Press, N.Y., 1976.

13. **Cess, R. D. and M. S. Lian**
A Simple Parameterization for Water Vapor Emissivity, *Trans. ASME J. Heat Transfer,* **98, 4,** 676-678, 1976.

14. **Edwards, D. K., Denny, V. E., and A. F. Mills**
Transfer Processes, Holt, Rhinehart and Winston, N.Y., 1973.

15. **Karlekar, B. V. and R. M. Desmond**
Engineering Heat Transfer, West Publishing Company, N.Y., 1977.

16. **Means, J. D., and R. D. Ulrich**
Transient Convective Heat Transfer During and After Gas Injection Into Containers *Trans. ASME J. Heat Transfer,* **97, 2,** 282-287, 1975.

17. **Siebers, D. L., Schwind, R. G., and R. J. Moffat**
Experimental Mixed Convection Heat Transfer From a Large, Vertical Surface in a Horizontal Flow, *Sandia National Laboratories,* Livermore, CA., SAND83-8225, 1983.

18. **Clausing, A. M. and S. N. Kempka**
The Influences of Property Variations on Natural Convection from Vertical Surfaces, *Trans. ASME J. Heat Transfer,* **103, 4,** 609-612, 1981.

19. **Kreith, F.**
Principles of Heat Transfer, 3rd Edition, International Textbook Company, Scranton, Pa., 1973.

20. **McAdams, W. H.**
Heat Transmission, 3rd Edition, McGraw-Hill Publishing Company, N.Y., 1954.

21. **Gebhart, B.**
Heat Transfer, 2nd Edition, McGraw-Hill Publishing Company, N.Y., 1971.

22. **Baer, M. R.**
A Theory of Droplet Combustion at High Pressures, *Sandia National Laboratories,* Albuquerque, N.M., SAND80-0081, 1980.

23. **Gunn, R., and G. D. Kinzer**
The Terminal Velocity of Fall for Water Droplets in Stagnant Air, *J. Meteor., 1949.*

24. **Harrje, D. T., ed.**
Liquid Propellant Rocket Combustion Instability, *NASA Publication,*NASA SP-194, 1976.

25. **White, F. M.**
Viscous Fluid Flow, McGraw-Hill Publishing Company, N.Y., 1974.

26. **Carnahan, B., Luther, H. A., and J. O. Wilkes**
Applied Numerical Methods, John Wiley and Sons, Inc., N.Y., 1969.

27. **Ratzel, A. C., Kempka, S. N., Shepherd, J. E. and A. W. Reed**
SMOKE: A Data Reduction Package for Analysis of Combustion Experiments, *Sandia National Laboratories,* Albuquerque, N.M., SAND83-2657, (in preparation).

28. **Bird, R. B., Stewart, W. E., and E. N. Lightfoot**
Transport Phenomena, John Wiley and Sons, Inc., N.Y., 1960.

29. **McCulloch, W.H., et al**
Hydrogen Burn Survival: Preliminary Thermal Model and Test Results, *Sandia National Laboratories,* Albuquerque, N.M., SAND82-1150, NUREG/CR-2730, 1982.

30. **Kempka, S. N., Ratzel, A. C., and M. R. Baer**
Multiple Hydrogen-Air Deflagrations in Containment and the Resulting Thermal Environments, *Proceedings of the Second International Conference on the Impact of Hydrogen on Water Reactor Safety,* Albuquerque, N.M., October 3-7, 1982.

NRC FORM 335 (2-84) NRCM 1102, 3201, 3202

U.S. NUCLEAR REGULATORY COMMISSION

BIBLIOGRAPHIC DATA SHEET

SEE INSTRUCTIONS ON THE REVERSE

1. REPORT NUMBER (Assigned by TIDC, add Vol. No., if any)
NUREG/CR-3779
SAND83-2579
Vol. 2

2. TITLE AND SUBTITLE
The Hydrogen Burn - Equipment Response Algorithm (HYBER) Reference Manual

3. LEAVE BLANK

4. DATE REPORT COMPLETED
MONTH: July YEAR: 1984

5. AUTHOR(S)
S.N. Kempka, A.C. Ratzel

6. DATE REPORT ISSUED
MONTH: August YEAR: 1984

7. PERFORMING ORGANIZATION NAME AND MAILING ADDRESS (Include Zip Code)
Sandia National Laboratories
P.O. Box 5800, Organization 1513
Albuquerque, NM 87185

8. PROJECT/TASK/WORK UNIT NUMBER

9. FIN OR GRANT NUMBER
A1306

10. SPONSORING ORGANIZATION NAME AND MAILING ADDRESS (Include Zip Code)
Division of Engineering
Office of Nuclear Reactor Regulation
U.S. Nuclear Regulatory Commission
Washington, D.C. 20555

11a. TYPE OF REPORT
Technical

b. PERIOD COVERED (Inclusive dates)

12. SUPPLEMENTARY NOTES

13. ABSTRACT (200 words or less)

The reference guide for HYBER (Hydrogen Burn - Equipment Response), the Hydrogen Burn Survival algorithm, is provided in this report. HYBER is comprised of two self-contained computer programs, DATGEN and SOLVER, developed on VAX 11/780 and CRAY-1 computer systems for use on IBM Personal Computers. These computer codes model single or multiple hydrogen:carbon monoxide:air combustion processes in single-volume vessels, providing predictions for the environment gase state and composition. HYBER was developed to model combustion processes in nuclear reactor containments and to estimate the thermal response of safety-related equipment subject to the combustion and post-combustion environments.

This reference guide discusses the combustion, heat, and mass transfer models included in the algorithm computer codes. The assumptions used in the codes and the execution procedure (i.e., computational framework) in SOLVER are provided. HYBER simulations of two experiments are compared with the data for two different vessels (5.6m^3 and 2084.m^3 total volume, respectively). These comparisons demonstrate the capabilities of modeling combustion processes with HYBER.

14. DOCUMENT ANALYSIS - a. KEYWORDS/DESCRIPTORS
HYBER
reference guide
equipment response

b. IDENTIFIERS/OPEN ENDED TERMS

15. AVAILABILITY STATEMENT
Unlimited

16. SECURITY CLASSIFICATION
(This page) Unclassified
(This report) Unclassified

17. NUMBER OF PAGES

18. PRICE

NUREG/CR-3779, Vol. 2

THE HYDROGEN BURN - EQUIPMENT RESPONSE ALGORITHM (HYBER) REFERENCE MANUAL

AUGUST 1984